



VCU

Virginia Commonwealth University
VCU Scholars Compass

Theses and Dissertations


Graduate School

2019

Theoretical Studies of the Structure and Stability of Metal Chalcogenide CrnTem ($1 \leq n \leq 6$, $1 \leq m \leq 8$) clusters

FNU Sweta Prabha
Virginia Commonwealth University

Follow this and additional works at: <https://scholarscompass.vcu.edu/etd>

 Part of the [Condensed Matter Physics Commons](#), [Other Physics Commons](#), and the [Quantum Physics Commons](#)

© The Author

Downloaded from

<https://scholarscompass.vcu.edu/etd/5774>

This Thesis is brought to you for free and open access by the Graduate School at VCU Scholars Compass. It has been accepted for inclusion in Theses and Dissertations by an authorized administrator of VCU Scholars Compass. For more information, please contact libcompass@vcu.edu.

Theoretical Studies of the Structure and Stability of Metal Chalcogenide Cr_nTe_m ($1 \leq n \leq 6$, $1 \leq m \leq 8$) clusters

A thesis submitted in partial fulfillment of the requirements for the
degree of Master of Science at Virginia Commonwealth University

By

Sweta Prabha

Int. Master of Technology, Nanotechnology, Central University of Jharkhand 2016

Primary Advisor: Dr. Shiv N Khanna, Professor, Department of Physics

Virginia Commonwealth University
Richmond, VA
Spring 2019

Acknowledgment

I would like to express my heartfelt gratitude to several people. I would like to thank my primary advisor Prof. Shiv N Khanna for his excellent leadership, patience and support. I wish to thank Dr. Loren Picco for having the kindness to let me work in his lab for a brief period of time which helped me build a foundation towards my career goals. I want to thank Dr. Arthur Reber without whom completion of this project would be next to impossible. I wish to thank my committee members Dr. Michael Reshchikov and Dr. Katherine Tibbetts for agreeing to be part of my advisory committee and making time out of their busy schedule to go over my thesis and dissertation. I would like to thank my fiancé Abhishek for undying support and faith in me. My parents deserve big thanks for their support and help without question. I also wish to thank Dr. Vikas and Dinesh for helping me in every way possible throughout my lab curriculum. My closest friends Adya, Nilufa and Hossain deserve a big Thank You for making my stay in Richmond much easier and comfortable. I wish to thank my course instructors Dr. Massimo Bertino, Dr. Everett Carpenter, Dr. Marilyn Bishop, Dr. Katherine Tibbetts and Dr. Loren Picco for challenging my mind throughout my curriculum. Lastly, I want to thank the entire VCU Physics Department for supporting me throughout my graduate study through Teaching Assistantship. Every member of the faculty and staff has gone through great lengths to help me reach my goals.

Sweta Prabha

TABLE OF CONTENTS

List of Figures

Abstract

I. Introduction

- 1.1: Background & Motivation 1
- 1.2: Objective 4

II. Computational Approach

- 2.1: Density Functional Theory 6
- 2.2: Theoretical Methods 12

III. Structure and Properties of Cr_nTe_m Clusters

- 3.1: Pure Chromium Clusters 15
- 3.2: Structures and Ground State Spins of Cr_nTe_m Clusters 17
- 3.3: HOMO-LUMO Gaps of Cr_nTe_m Clusters 23
- 3.4: Fragmentation and Binding Energies of Cr_nTe_m Clusters 25
- 3.5: Ionization Potential and Electron Affinity of Cr_nTe_m Clusters 27
- 3.6: d-orbital Occupation of Cr_nTe_m Clusters 29

IV. Stable Clusters: Cr_4Te_6 and Cr_6Te_8

- 4.1: Electronic and Chemical Properties of Cr_4Te_6 Cluster 31
- 4.2: d-Orbital Splitting of Cr in Cr_4Te_6 Cluster 32

4.3: Electronic and Chemical Properties of Cr_6Te_8 Cluster	34
4.4: d-Orbital Splitting of Cr in Cr_6Te_8 Cluster	35
V. Discussion & Conclusion	40
VI. Summary & Future Direction	44
VII. Bibliography & References	45

LIST OF FIGURES

Figure 1 :	Examples of synthesized ligated Metal-chalcogenide clusters	3
Figure 2 :	Cluster Assembled Materials of metal chalcogenide clusters with C_{60}	3
Figure 3 :	Bond-Distance vs Binding Energies of Cr-dimer for antiferromagnetic (A) , ferromagnetic (B) and excited (C) states a) Previously Reported b) calculated using PBE0 functional c) calculated using PBO functional	14
Figure 4 :	Structure and magnetic properties of pure Cr_n (n=1-6) clusters	16
Figure 5 :	Structure, Magnetic spin and average bond distances of Cr_nTe_m clusters (n=1-6, m=1-8)	21
Figure 6 :	Spin Magnetic Moment (μ_b) of Cr_nTe_m clusters (n=1-6, m=1-8)	22
Figure 7 :	HOMO-LUMO gaps of Cr_nTe_m clusters (n=1-6, m=1-8)	24
Figure 8 :	Fragmentation Energies of Cr_nTe_m clusters (n=1-6, m=1-8)	26
Figure 9 :	A) Ionization Energies of Cr_nTe_m clusters (n=1-6, m=1-8) B) Electron Affinities of Cr_nTe_m clusters (n=1-6, m=1-8)	28
Figure 10 :	3d Occupation of Cr atoms in the up and down channel of Cr_nTe_m clusters (n=1-6, m=1-8)	29
Figure 11 :	The ligand field splitting of Cr_6Te_8 . The red percentages give the percent of the orbital corresponding to the Cr 3d orbital	33
Figure 12 :	The structure, spin magnetic moment, ionization energy and electron affinity of $Cr_6Te_8(PEt_3)_6$	39

LIST OF ABBREVIATIONS

DFT :	Density Functional Theory
ADF :	Amsterdam Density Functional
GGA :	Generalized Gradient Approximation
PBE :	Perdew-Burke-Ernzerhof
XC :	Exchange Correlation
HOMO :	Highest Occupied Molecular Orbital
LUMO :	Lowest Unoccupied Molecular Orbital
AIP/AIE :	Adiabatic Ionization Potential/Ionization
AEA :	Adiabatic Electron Affinity
CAMs :	Cluster Assembled Materials
LCAMs :	Ligated Cluster Assembled Materials
FE :	Fragmentation Energy

ABSTRACT

Theoretical Studies of the Structure and Stability of Metal Chalcogenide $Cr_n Te_m$ ($1 \leq n \leq 6$, $1 \leq m \leq 8$) clusters

By Sweta Prabha

A thesis submitted in partial fulfillment of the requirements for the degree of Master of Science at Virginia Commonwealth University.

Virginia Commonwealth University, 2019

Major Director: Prof. Shiv N. Khanna

In the presented work, first principle studies on electronic structure, stability, and magnetic properties of metal chalcogenide, $Cr_n Te_m$ clusters have been carried out within a density functional framework using generalized gradient functions to incorporate the exchange and correlation effects. The energetic and electronic stability was investigated, and it was found that they are not always correlated as seen in the cluster $Cr_6 Te_8$ which has smaller gap between its HOMO (Highest Occupied Molecular Orbital) and LUMO (Lowest Unoccupied Molecular Orbital) and a high electron affinity of 3.39 eV indicating lower electronic stability whereas higher fragmentation energy indicating energetic stability. The high electron affinity shows that the stability of $Cr_6 Te_8$ cluster can be enhanced by adding charge donating ligands including PEt_3 to form stable $Cr_6 Te_8(PEt_3)_6$ clusters as seen in experiments^{1,2}. The other cluster of interest was $Cr_4 Te_6$ in which energetic stability was accompanied with electronic inertness marked by its large HOMO-LUMO gap, non-magnetic ground state and high fragmentation energy.

I. INTRODUCTION

1.1 Background and Motivation

Atomic clusters are the novel frontier of solid-state physics that provides unique properties different from bulk solids. In the past few decades, there has been advancement in experimental techniques enabling researchers to synthesize sub-nanoscale clusters containing few to a thousand atoms. These nanoclusters display distinct properties from their bulk behavior. For example, gold in its bulk form is a noble metal whereas in its cluster form it serves as an excellent catalyst and hence is highly reactive³. The concept of stable clusters was generated from the idea of magic clusters. Knight et al.⁴ showed that for clusters of Sodium containing N atoms, the mass spectra show large peaks at N = 8, 20, 40, 58 and 92 which implies clusters of these sizes are more stable than their neighboring sizes. It was realized that these numbers could be understood within a model of a confined nearly free electron gas. In this model states are grouped into electronic levels for clusters corresponding to $1S^2 1P^6 1D^{10} 2S^2 1F^{14} 2P^6 \dots$ which is analogous to atomic levels in atoms. It is found that chemical properties of several metallic clusters can be predicted by using Shell model. As seen by experiments on Aluminum clusters, structures with closed shells are more stable⁵. With the knowledge of this new area involving interaction between atoms in nanoscale, a huge scope of study and synthesis of nanoclusters came into existence. The structures and properties could be optimized by changing the element or group of elements. The type and arrangement of atoms governed the physical properties including magnetic, optical, mechanical properties and the reactivities of these structures. The identification of stable clusters opened the possibility of using these as building blocks of new three-dimensional solids called Cluster-Assembled Materials (CAMs)^{6,7}. In the past two decades,

attempts has been made to devise cluster assembled materials and investigate their properties both theoretically and experimentally. Density Functional Theory is a significant tool for determining the properties of these CAMs theoretically. One of the key propositions is to understand the transformation of properties as nanostructures build upward from individual motifs termed as “bottom-up” approach. For small sizes, grouping of electronic states take place into orbital shells and the stability of the structure depends on filling of these orbital shells. This idea of constructing custom materials using CAMs as the building blocks offers a huge prospect to form various class of cluster systems. In this study, one such class namely, metal-chalcogenide cluster has been investigated. The term chalcogenide refers to dianionic elements from group 16 (VIA), of the periodic table; namely, sulfur, S^{2-} ; oxygen, O^{2-} ; selenium, Se^{2-} ; and tellurium, Te^{2-} . Covalent Bonds between metals and chalcogen forms a material which possesses broad valence and conduction bands while maintaining a band gap (d-orbital of metals mix with s- and p- orbitals of chalcogen and lift its degeneracy). Experiments^{2,8} have shown that pairing chalcogens with transition metals give rise to stable clusters with interesting optical, magnetic and electronic properties all sensitive to impurities/vacancies. Thus metal-chalcogenide clusters form a new class of superatoms with promising properties. Since these clusters were sensitive to impurities or vacancies, there was room for capping them with ligands and studies² showed that ligated metal chalcogenide clusters displayed phenomenal properties. As seen in the case of $Ni_9Te_6(PEt_3)_8$ (ligated metal-chalcogenide clusters), which behaves as excellent charge donor and can donate charge to C_{60} which is a slightly acceptor material to form ionic crystal. This phenomenon was explained by Chauhan et al⁹ as the charge transferred from PEt_3 to Ni_9Te_6 created an internal, coulombic potential well that lifts the quantum states of the cluster lowering its ionization potential. Figure 1 shows few experimentally synthesized ligated metal-chalcogenide clusters whereas Figure 2 shows the structures of metal chalcogenide materials

formed by the anchoring of ligated clusters with C_{60} .

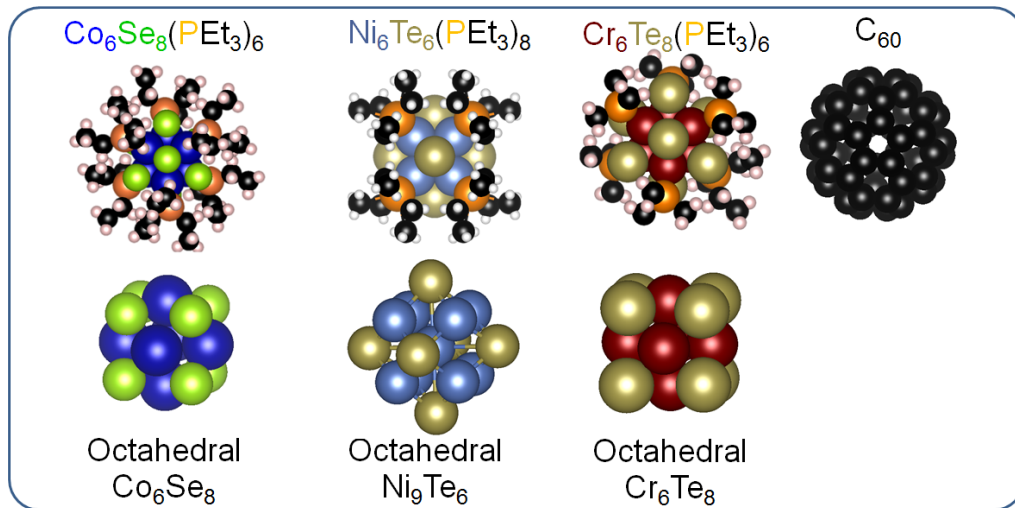


Figure 1 :
Examples of synthesized ligated Metal - chalcogenide clusters

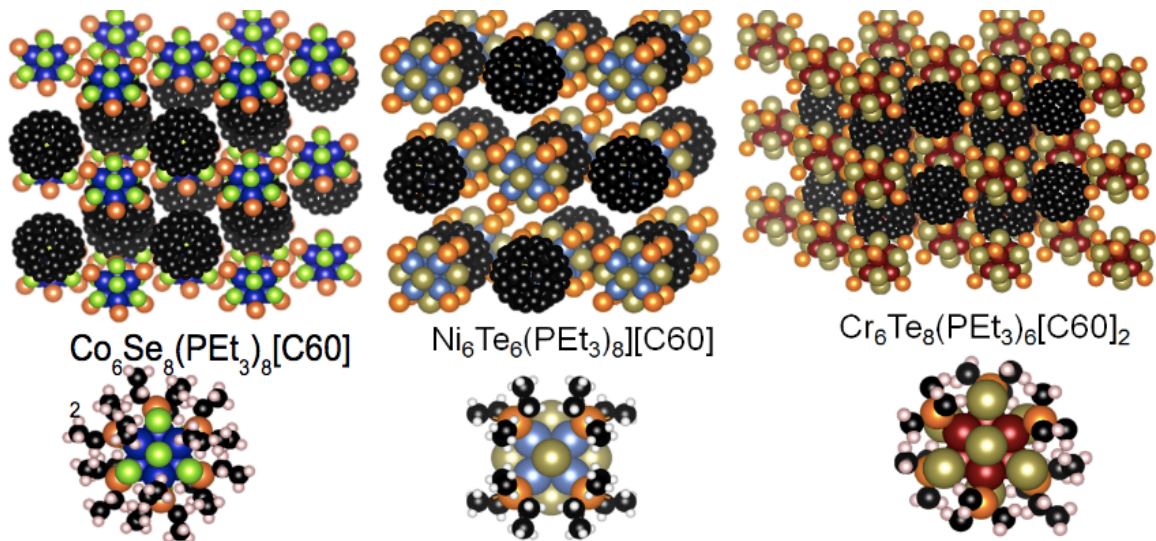


Figure 2 :
Cluster Assembled Materials of metal chalcogenide clusters with C_{60}

1.2 Objectives

The objective of this current study is to explore Chromium-Tellurium metal chalcogenide clusters. Chromium is a group 6 element with atomic number 24. It comes under the category of transition metals with half-filled d-orbital that is responsible for its remarkable magnetic properties. It is the only known element that shows antiferromagnetic ordering at room temperature. It can pair up with chalcogenide metals to give various clusters with inordinate physical and chemical properties. Tellurium belongs to the chalcogenide group. An atom has the tendency to follow the 8-N rule which refers to the number of single covalent bonds it requires to complete its outer shell. Tellurium is no exception to it and possesses 8-N rule dependency and this property can be exercised to form novel cluster materials. High spin 3-d transition metals paired with chalcogenides involves mixing between d-orbitals of metal and s and p orbital of the chalcogen which results in lifting of degeneracy and the separation between orbitals can be manipulated by optimizing the geometric structures. Metal Chalcogenide systems like Cobalt-Selenium, Cobalt-Tellurium, Molybdenum-Selenium and Nickel-Tellurium has been widely studied and synthesized whereas relatively little information is available about Chromium-Tellurium clusters. There has been conflicting experimental studies on $\text{Cr}_6\text{Te}_8(\text{PEt}_3)_6$ clusters with one experiment identifying it as ferrimagnetic and the other as antiferromagnetic. Electronic structures of Chromium-Tellurium systems are interesting. Congener $\text{Mo}_6\text{Se}_8(\text{PEt}_3)_6$ ⁸ is nonmagnetic with large HOMO-LUMO gap, while chromium-based clusters appear to have local moments. Chromium based clusters also have close lying isomers and the magnetic moment is affected by changing the ligand or charge state. All these information leads to inquisitive focus of many researchers towards Chromium based clusters. Experimental findings¹⁰ of electronic and chemical properties of Chromium-Oxygen clusters agreed with the predicted results

of theoretical Density Functional Theory calculations and based on this notion, the systematic study of pure Chromium, Chromium-Tellurium and Ligated Chromium Tellurium clusters has been carried out theoretically within density functional framework.

II. COMPUTATIONAL APPROACH

2.1 Density Functional Theory

Density functional theory is one of the most popular and successful quantum-mechanical approaches in studying solid state physics and cluster systems⁶². It can be applied to calculate binding energy of clusters and band structures. Two core theorems of DFT are i) the Hohenberg-Kohn theorem and ii) Kohn-Sham equations.

In quantum mechanics, we all learnt that all information we can possibly have about a given system of electrons in atoms, molecules and solids is contained in its wave function that is denoted by ψ . The nuclear degrees of freedom appear in the form of a potential $v(r)$ acting on the electrons. This wavefunction is calculated from Schrodinger's equation which for a single electron with potential $V(r)$ is given by,

$$\left[-\frac{i\hbar}{2m}\nabla^2 + V(\vec{r})\right]\psi(\vec{r}) = \epsilon\psi(\vec{r}) \quad (1)$$

which in Hamiltonian operator form is written as,

$$\hat{H}|\psi\rangle = E|\psi\rangle \quad (2)$$

If there are more than one nuclei, it becomes a many body problem,

However, the motion of nuclei and electrons can be separated using the Born-Oppenheimer approximation that simplifies the problem allowing treatment of electronic degrees of freedom for fixed position of nuclei. In Born-Oppenheimer approximation, Schrodinger equation is given by,

$$\left[\sum_{i=1}^N -\frac{1}{2}\nabla_i^2 + \sum_{A=1}^M \hat{V}_{\text{ext}}(r_i) + \sum_{i=1}^N \sum_{j>i}^N \hat{V}_{ee}(r_i, r_j)\right]\psi = E\psi \quad (3)$$

where the first term is the kinetic energy operator, second and third term are nucleus-electron interaction potential and the repulsive electron-electron potential operators respectively. ψ is the N-electron wavefunction. Equation (4) can be solved in two ways, *Hartree-Fock Approximation* and *Density*

Functional Theory:

Hartree-Fock (HF) approximation:

The solution of the Schrodinger equation involving electronic Hamiltonian is the wavefunction, ψ_e that depends on the position of electrons and nuclei

$$\psi_e = \psi(\{\vec{r}_i\}, \{\vec{R}_A\}) \quad (5)$$

Spin is another important quantity in describing the properties of electrons. Two quantities spin up ($\alpha(s)$) and spin down ($\beta(s)$) exists, where both of these are functions of variable s. Each electron can thus be represented by two quantities,

$$\vec{x} = \{\vec{r}, s\} \quad (6)$$

The wavefunctions in molecular electronic structure is described by a molecular orbital. A spatial orbital $\psi_i(\vec{r})$ describes the distribution of an electron at position so that the probability of finding that electron in a region $d\vec{r}$ is 1. The addition of spin takes the spatial orbital to a spin orbital which is defined for one electron as,

$$\chi(\vec{x}) = \begin{cases} \psi(\vec{r})\alpha(s) \\ \psi(\vec{r})\beta(s) \end{cases} \quad (7)$$

For N-electron system, the fully anti-symmetrized determinant wavefunction that minimizes the total energy of a fully interacting Hamiltonian is given by,

$$\psi_{HF}(\vec{x}_1, \vec{x}_2, \dots, \vec{x}_N) = (N!)^{-1/2} \begin{vmatrix} \chi_i(\vec{x}_1) & \chi_j(\vec{x}_1) & \dots & \chi_k(\vec{x}_1) \\ \chi_i(\vec{x}_2) & \chi_j(\vec{x}_2) & \dots & \chi_k(\vec{x}_2) \\ \vdots & \vdots & \ddots & \vdots \\ \chi_i(\vec{x}_N) & \chi_j(\vec{x}_N) & \dots & \chi_k(\vec{x}_N) \end{vmatrix} \quad (8)$$

where, $(N!)^{-1/2}$ is the normalization constant. The matrix and its solution are called Slater Determinant and the procedure is called *Hartree-Fock Approximation* (HF).

when the Hartree product is antisymmetrized to obtain the Slater determinant, exchange effect is seen.

Density Functional Theory is governed by two underlying theorems, *Hohenberg-Kohn Theorem* and *Kohn-Sham Theorem*,

Hohenberg-Kohn Theorem

First Hohenberg Kohn -Theorem: First theorem states that the ground state electron density $\rho(\vec{r})$ of an electronic system uniquely determines the external potential acting on the electrons up to an additive constant.

The external potential V_{ext} is determined, within a trivial additive constant, by the ground state electron density, $\rho(\vec{r})$. This tells us that the wave function can be determined from the ground state electron density along with all other properties of the system. It is concluded that same ground state electron density cannot correspond to two different external potential. The ground state electron density determines the total number of electron through,

$$N = \int \rho(\vec{r}) d\vec{r} \quad (9)$$

Hence, $\rho(\vec{r})$ uniquely determines the Hamiltonian via N and V_{ext} .

The second Hohenberg-Kohn theorem states that, once the Hamiltonian is known using the first theorem, in principle, the wavefunction of any state can be obtained by solving the Schrodinger equation. Consequently the ground state wavefunction along with all the ground state properties such as kinetic and potential energies are uniquely determined by the ground state electron density, $\rho(\vec{r})$. Thus for a given external potential the total energy becomes a functional of $\rho(\vec{r})$ as follows,

$$E[\rho] = T[\rho] + V_{\text{ee}}[\rho] + \int \rho(\vec{r})v(\vec{r}) d\vec{r} = F_{HK}[\rho] + \int \rho(\vec{r})v(\vec{r}) d\vec{r} \quad (10)$$

where $F_{HK}[\rho]$ is the Hohenburg-Kohn functional which is the combination of kinetic energy ($T[\rho]$) and Coulomb repulsion ($V_{\text{ee}}[\rho]$).

This theorem provides a variational principle with $\rho(\vec{r})$ as the basic variable to solve for $E[\rho]$. It says

that for a given trial density $\tilde{\rho}(\vec{r})$ with constraints $\int \tilde{\rho}(\vec{r}) d\vec{r} = N$ and $\tilde{\rho}(\vec{r}) \geq 0$, total energy function will be given by,

$$E_0 \leq E_v[\tilde{\rho}] \quad (11)$$

where, $E_v[\tilde{\rho}]$ is the energy functional of,

$$E_v[\tilde{\rho}] = T[\tilde{\rho}] + U_{ne}[\tilde{\rho}] + V_{ee}[\tilde{\rho}] = \int \tilde{\rho}(\vec{r}) v(\vec{r}) d\vec{r} + F_{HK}[\tilde{\rho}] \quad (12)$$

with,

$$F_{HK}[\rho] = F[\rho] = T[\rho] + V_{ee}[\rho]$$

where $F_{HK}[\rho]$ is the Hohenberg-Kohn functional which is the combination of kinetic energy ($T[\rho]$) and Coulomb repulsion ($V_{ee}[\rho]$). Thus assuming $E[\tilde{\rho}]$ is differentiable, the two theorems yield the fundamental expression of DFT. The electron density which minimizes $E[\rho]$ is obtained via stationary principle,

$$\delta[E[\rho] - \mu \left(\int \rho(\vec{r}) d\vec{r} - N \right)] = 0 \quad (13)$$

where μ is Lagrange multiplier for the constraint $\int \rho(\vec{r}) d\vec{r} = N$, called chemical potential. The above expression tells us that the ground-state energy and its density are the minimum to some functional $E[\rho]$. Eq. (13) yields the value of μ at the minimum for a constraint minimization,

$$\mu = V_{ext} + \frac{\delta F_{HK}}{\delta \rho(\vec{r})} \quad (14)$$

In the HK theorems, we learnt about the possibility of calculating ground state properties by knowing the ground state electron density.

Kohn-Sham method:

The Kohn-Sham method provides the computational scheme to calculate ground state electron density, $\rho(\vec{r})$. There are a set of Kohn-Sham equations that are solve self consistently to obtain $\rho(\vec{r})$ that minimizes $E[\rho]$.

First a non interacting N-electron system with the same electron density as the real system of inter-

est is defined for reference. The Hamiltonian for such system can be written as,

$$\hat{V} = \sum_{i=1}^N -\frac{1}{2} \nabla_i^2 + \sum_{A=1}^M v_s(\vec{r}_i) = \sum_{i=1}^N \hat{h}_i \quad (15)$$

where, \hat{h}_i is the single electron Hamiltonian and $v_s(\vec{r}_i)$ is single-electron potential. For this system the ground state wavefunction can be given by a Slater type determinant of the N lowest energy states.

Its kinetic energy can be calculated exactly and is given by,

$$\begin{aligned} T_{ks}[\rho] &= -\left\langle \psi_s \left| \sum_{i=1}^N \frac{1}{2} \nabla_i^2 \right| \psi_s \right\rangle \\ &= -\sum_{i=1}^N \left\langle \psi_i \left| \frac{1}{2} \nabla^2 \right| \psi_i \right\rangle \end{aligned} \quad (16)$$

where ψ_i 's represent the single electron orbitals and are eigenstates of one electron Hamiltonian \hat{h}_i .

As electron-electron interactions are absent, the kinetic energy functional (TKS $[\rho]$) of the reference system is not equal to T $[\rho]$ of the interacting system. Kohn and Sham wrote E $[\rho]$ in the following form Kohn and Sham wrote E $[\rho]$ in the following form,

$$E[\rho] = T_{ks}[\rho] + J[\rho] + E_{xc}[\rho] + \int \rho(\vec{r}) V_{ext} d\vec{r} \quad (17)$$

Here, J $[\rho]$ is the classical electron-electron repulsion energy and $E_{xc}[\rho]$ is called Exchange-Correlation function given by,

$$E_{xc}[\rho] = (T[\rho] - T_s[\rho]) + (V_{ee}[\rho] - J[\rho]) \quad (18)$$

Using stationary principle (Eq. 13), a condition on $\rho(\vec{r})$ that minimizes E $[\rho]$ is given by,

$$\mu = V_{ext} + \frac{\delta J[\rho]}{\delta \rho(\vec{r})} + \frac{\delta E_{xc}[\rho]}{\delta \rho(\vec{r})} + \frac{\delta T_{ks}[\rho]}{\delta \rho(\vec{r})} \quad (19)$$

From Eq. (14) and (19),

$$\begin{aligned} v_s &= V_{ext} + \frac{\delta J[\rho]}{\delta \rho(\vec{r})} + \frac{\delta E_{xc}[\rho]}{\delta \rho(\vec{r})} \\ &= V_{ext} + \int \frac{\rho(\vec{r}')}{|\vec{r} - \vec{r}'|} d\vec{r}' + V_{xc} \end{aligned} \quad (20)$$

where , exchange correlation potential is defined as follows,

$$V_{xc} = \frac{\delta E_{xc}[\rho]}{\delta \rho(\vec{r})} \quad (21)$$

Thus, we can see that the problem of interacting N-electron system under V_{ext} is mapped into a problem of non-interacting electrons moving under an effective potential of $V_{eff} = v_s(\vec{r})$. Thus, the set of N-single electron equation are known as Kohn-Sham equations and is given as,

$$\left[-\frac{1}{2} \nabla_i^2 + \hat{V}_{eff}(\vec{r}_i) \right] \psi_i = \epsilon_i \psi_i \quad (22)$$

The ground state electron density and single electron Kohn-Sham orbitals are related as follows,

$$\rho(\vec{r}) = \sum_{i=1}^N |\psi_i(\vec{r})|^2 \quad (23)$$

Eq. (20) and Eq. (22) are solved self consistently to obtain Kohn Sham orbitals ψ_i 's under the constraint in Eq. (23). The total energy in Kohn Sham formalism is written as,

$$E[\rho] = \left\langle \psi_i \left| -\frac{1}{2} \nabla_i^2 + V_{eff}(\vec{r}_i) \right| \psi_i \right\rangle + \int \frac{\rho(\vec{r}_1)\rho(\vec{r}_2)}{|\vec{r}_1 - \vec{r}_2|} d\vec{r}_1 d\vec{r}_2 + E_{xc}[\rho] + \int \rho(\vec{r}) V_{ext} d\vec{r} \quad (24)$$

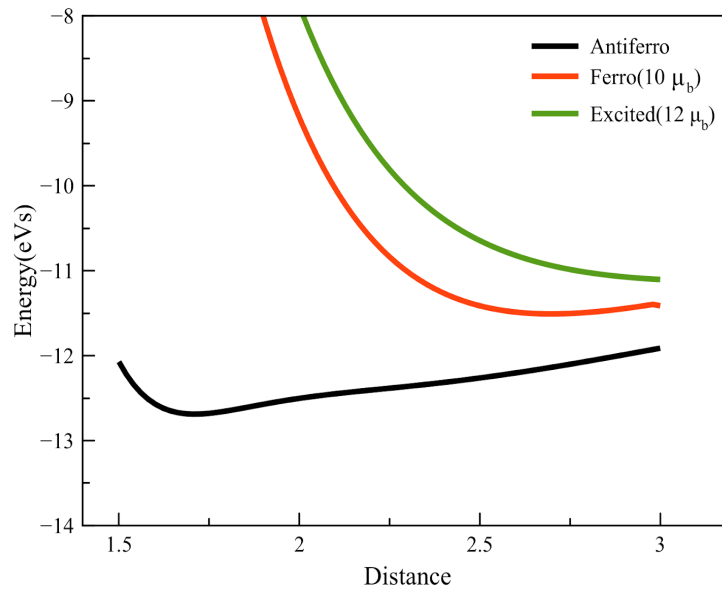
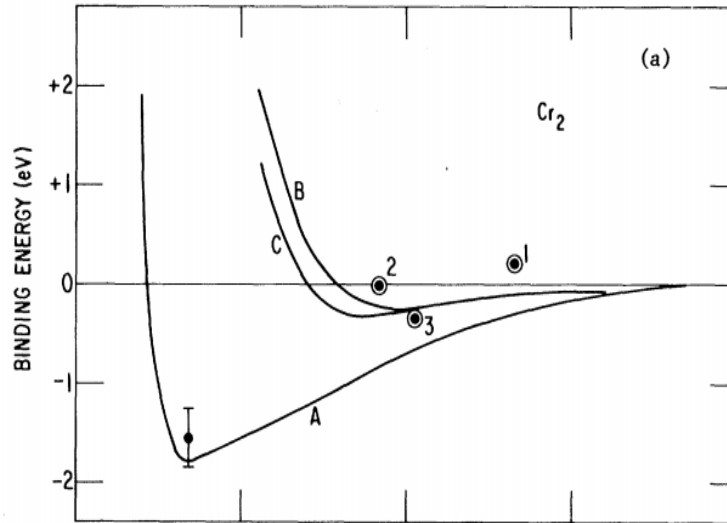
This is solved self consistently by starting with some trial charge density and generating V_{eff} . Then we solve the Kohn-Sham equations to get ψ_i 's and calculate $\rho(\vec{r})$. This process is repeated until the output charge density and energy are same as input values.

In DFT, ground state energy can be calculated using a functional expression for Exchange-correlation

2.2 Theoretical Methods

First Principle electronic structure studies has been carried out using the Amsterdam Density Functional (ADF) set of codes¹¹. An exchange and correlation functional based on generalized gradient approximation (GGA) as proposed by Perdew, Burke, and Ernzerhof (PBE)¹² is found to give reasonable estimates of the experimentally available binding energy and electronic properties of related systems. In the ADF code, the electronic wave function of the cluster is formed by a combination of Slater-type orbitals (STO) centered at the atomic sites and the cluster wave functions are created from a linear combination of these atomic orbitals. A TZ2P basis set and a small frozen electron core has been used. In all cases, the total energies and the forces at the atomic sites are computed and the local ground state for each structure is obtained by using quasi-Newton method without any symmetry restriction. In each step, the zero-order regular approximation (ZORA) is used to incorporate scalar-relativistic effect¹³. The calculations covered the neutral as well cationic species, and several possible spin multiplicities and local orientation of spins were considered to find the ground state. To validate this methodology, calculations were performed on Cr_2 , Cr_2^+ , Cr_6 , Cr_2O and Cr_2O_2 clusters for which experimental data on the bond length, binding energy, and electron binding energy are available. Oxygen was chosen because no data could be found for Cr-Te clusters, and O and Te belong to the same column of the periodic table. Fig 3 compares the bond distance of Cr dimer calculated using PBE and PBE0 functional with the reported data. Table 1 compares the calculated values using the PBE and PBE0 functionals with experimental values. Here, IP represents the adiabatic ionization energy, VDE represents the vertical detachment energy obtained by the energy difference between the ground state of the anion and the neutral in the same geometry as anionic ground state, while EA represents the adiabatic electron affinity representing

the difference between the ground state energy of anion and that of the neutral cluster. The VDE corresponds to the first peak in the photo-detachment spectra of the anionic clusters. Note that the PBE functional provides a much better representation of the available experimental data and is used in the remainder of this work.



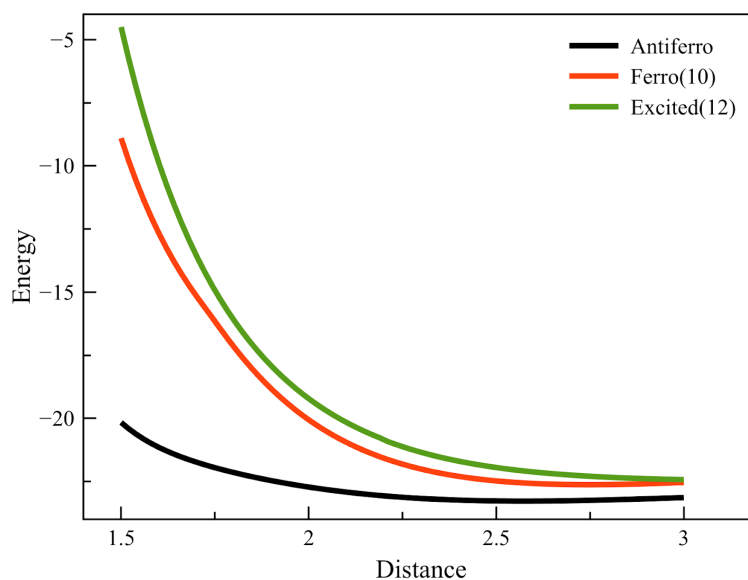


Figure 3 : Bond - Distance vs Binding Energies of Cr - dimer for antiferromagnetic, ferromagnetic and excited states (a) Previously Reported¹⁴ (b) calculated using PBE0 functional (c) calculated using PBE functional

Cluster	Exp.	PBE	PBE0
Cr ₂ Bond Dist.	1.68 Å ¹⁵	1.70 Å	2.50 Å
Cr I.P.	6.77 eV	7.38 eV	7.07 eV
Cr ₂ I.P.	6.4 ± 0.2 eV ¹⁶ 6.89 ± 0.08 eV ¹⁷	7.37 eV	6.40 eV
Cr ₂ ⁺ B.E.	1.3 eV ¹⁸	1.70 eV	1.52 eV
Cr ₂ B.E.	1.42 ± 0.10 eV ¹⁸ 1.443 ± 0.05 eV ¹⁷	1.62 eV	0.85 eV
Cr ₂ O VDE	1.10 eV ¹⁹	0.98 eV	0.70 eV
Cr ₂ O ₂ VDE	1.67 eV ¹⁹	1.10 eV	1.07 eV
Cr ₆ VDE	2.0 eV	1.60 eV	1.78 eV
Cr ₆ VDE	1.9 eV ²⁰	1.51 eV	1.50 eV

Table 1. Relevant experimental measurements, and calculated results using PBE, and PBE0 functionals.

III. Structure and Properties of Cr_nTe_m Clusters

3.1 Pure Chromium Clusters

In the present work, a systematic study of pure chromium cluster from sizes Cr_n ($n=1-6$) has been carried out and the effect of adding Tellurium atoms on the physical and chemical properties were analyzed. Figure 4 shows the structure, spins and average bond lengths of pure chromium clusters. A single chromium atom has a spin magnetic moment of $6 \mu_B$. It possesses a ground state of 7S_3 , in a $3d^54s^1$ configuration²¹. The bond-length of Cr_2 dimer is found to be 1.68 \AA ⁴² which is in good agreement with the calculated value in the present study. This value is drastically shorter than the Cr-Cr bond-length in bulk which is 2.50 \AA ²². Chromium atom has six unpaired electron and ideally it should produce a dimer with six bonds but in this case the binding energy is too low ($1.53 \pm 0.05 \text{ eV}$)²³. The small value of binding energy is assumed to be the result of size difference between 4s and 3d orbitals as well as influence from exchange energy. The ionization potential and binding energy calculated in the present investigation are 7.37 eV and 1.62 eV respectively which are in fair agreement with the experimental values of $6.89 \pm 0.08 \text{ eV}$ ¹⁷ and $1.44 \pm 0.05 \text{ eV}$ ¹⁷ respectively. The Cr-Cr bond-length increases with addition of chromium atoms. Chromium trimer is ferrimagnetic with local spins $5.0 \mu_B$, $5.0 \mu_B$ and $-4.0 \mu_B$ in its three atoms with a septuplet spin and magnetic moment of $6 \mu_B$ which was claimed in the work of Lopez-Estrada et. al.²⁴ The Chromium tetramer is deemed antiferromagnetic with an average bond length of 2.35 \AA . The local spins on each chromium atoms were found to be $4.7 \mu_B$ and $-4.7 \mu_B$. It forms a planar rhombus structure and on addition of

another chromium, that is chromium pentamer forms a distorted tetragonal bipyramidal structure with an average bond length of 2.39 Å, almost close to chromium tetramer. The ground state of Cr₆ is antiferromagnetic with a structure resembling a distorted octahedron. The average bond length is about 2.38 Å. Further, addition of Tellurium atoms to these pure clusters effect both the structure and properties of the clusters. In the course of this thesis, the effect of adding tellurium to pure chromium has been explored by means of theoretical calculations.

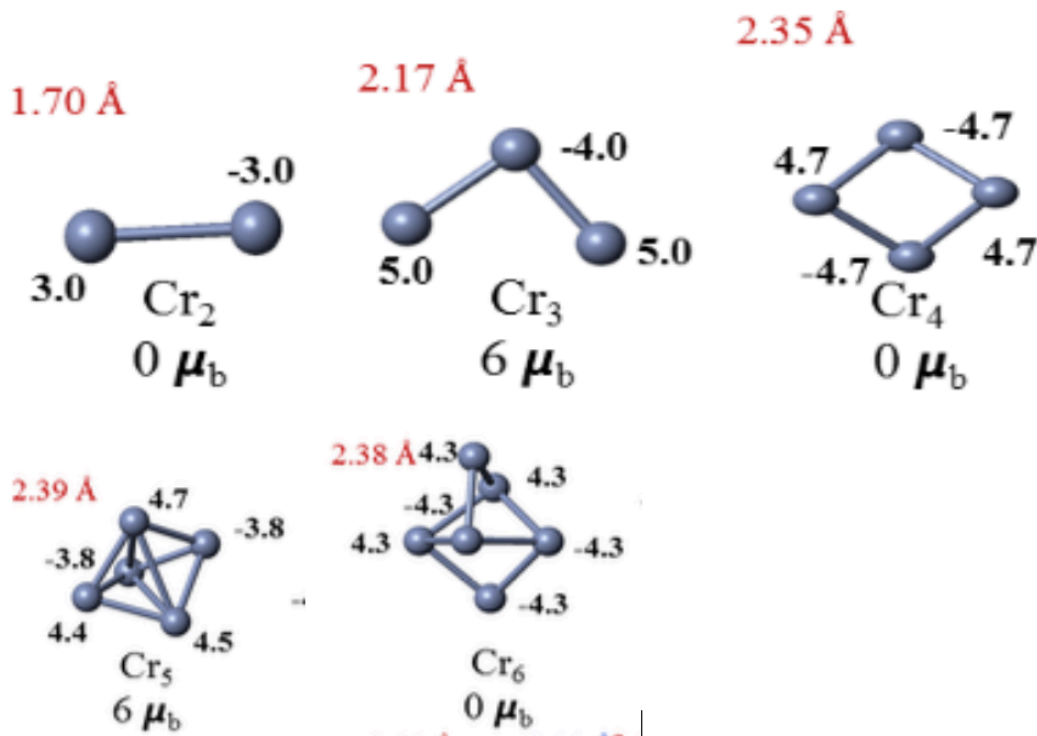


Figure 4 :
Structure and magnetic properties of pure Cr_n (n = 1 - 6) clusters

3.2 Structures and Ground State Spins of Cr_nTe_m Clusters

Figure 5 and 6 shows the ground state geometries and total magnetic spins of Cr_nTe_m clusters, $n=1-4$, and $m=0-6$. The local spin magnetic moments at the chromium and Tellurium site has been shown with progression of geometry as the Te atoms are added one at a time. The nature of coupling is shown as Te atoms are added.

The average Cr-Cr and Cr-Te bond-lengths and the overall spin magnetic moment of the cluster has been indicated. The total magnetic moment of the cluster is the integral sum of all the spin up and spin down magnetic moment in a sphere around the metallic sites. As we have seen previously, the spin magnetic moment of Cr atom is $6 \mu_B$. When the first tellurium atom is added, the moment is lowered to $4 \mu_B$ with chromium site showing a local spin moment of $4.8 \mu_B$. There is no further change in overall moment up to three tellurium atoms. The net moment is still $4 \mu_B$ with Cr sites possessing local spin moments of $4.6 \mu_B$ and $4.5 \mu_B$ for two and three Te atoms respectively. The lowering of net magnetic moment is due to the opposite polarization of tellurium atoms in CrTe_m clusters. When the fourth tellurium atom is added, the net moment is further reduced to $2 \mu_B$. Chromium dimer is antiferromagnetic with local moments of $3.0 \mu_B$ as reported by previous studies¹⁴ and addition of one Te atom doesn't make much difference in terms of net magnetic moment of the cluster. However, the bond-distance of Cr dimer is stretched from 1.70 \AA to 2.62 \AA . This increase in bond-length is presumably because the Te atom mediate the interaction between multiple Cr atoms which effect is also reflected in Cr_2Te_2 both in bond distance and net magnetic moment. The average bond distance between chromium atoms in Cr_2Te_2 is 2.57 \AA . There is a drastic change in

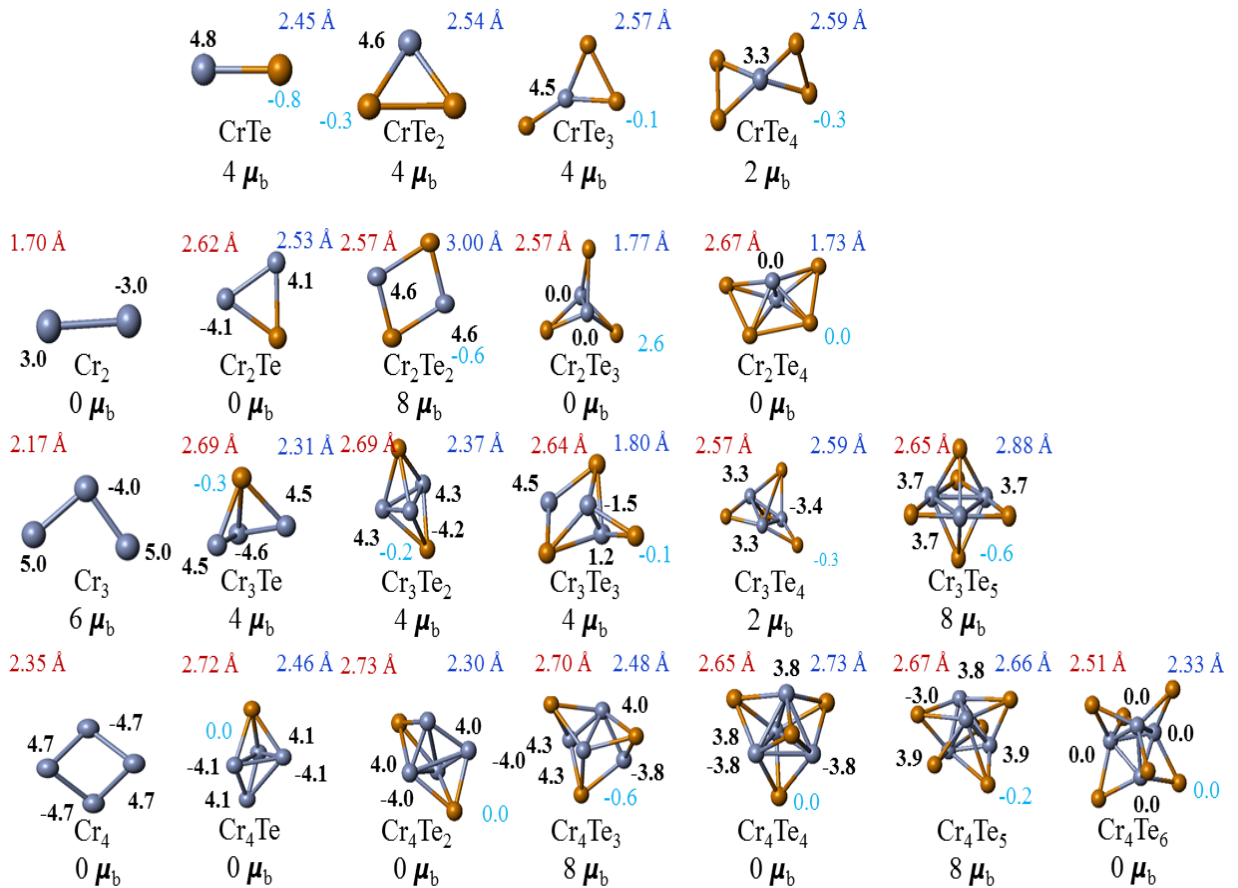
magnetic moment with addition of two tellurium atoms. Cr_2Te_2 is ferromagnetic with a net magnetic moment of $8 \mu_B$ due to the bridging by Tellurium atoms between two chromium atoms which leads to super-exchange interaction across chromium sites. Addition of third and fourth Te atoms renders the cluster non-magnetic which refers to quenching of the local spins of Cr sites by Te atoms. There is no visible change in average Cr-Cr bond distance in Cr_2Te_3 and Cr_2Te_4 clusters. It can be concluded that addition of tellurium atoms in a pure Cr cluster changes the magnetic spins due to the modification of the structure and mediation of Te atoms carrying $-0.6 \mu_B$ spins in between Cr pairs. The ground state of chromium trimer is ferrimagnetic with two chromium atoms having spin moments of $5.0 \mu_B$ and $-4.0 \mu_B$. The geometry of Cr_3 cluster is an obtuse angled triangle with two end Cr sites aligned with local moments of $5.0 \mu_B$. With addition of 1, 2 and 3 Te atoms, the magnetic moments were reduced to $4 \mu_B$. All these three clusters had Cr_3 cores with frustrated spin moments with two chromium atoms as spin up and the third one antiferromagnetically aligned with spin down. The local spin of Cr atoms in Cr_3Te_4 is further quenched with a net moment of $2 \mu_B$. There was a rise in spin magnetic moment seen for Cr_3Te_5 cluster. In this cluster, the moments on all the Cr sites are ferromagnetically aligned. In the Cr_3 series the average Cr-Cr bond length increased from 2.17 \AA to 2.69 \AA from Cr_3 to Cr_3Te . There is not much stretching seen thereafter and the average bond length lied between 2.57 to 2.69 \AA . Cr_3 forms the triangular core and the Te atoms are all three coordinated with the Cr atoms except Cr_3Te_4 , which had two coordinated Te atoms. The ground state of Cr_4 cluster is a rhombus structure that has antiferromagnetically linked Cr sites with no net magnetic moment. This antiferromagnetic coupling persists upto the addition of one and two Te atoms, but the average Cr-Cr bond length is stretched with introduction of Te atoms. The average bond length in Chromium tetramer is 2.35 \AA and is increased to 2.72 \AA in Cr_4Te and 2.73 \AA

in Cr_4Te_2 , Cr_4Te_3 and Cr_4Te_4 clusters, the effect of Te is seen in terms of increased moment. The net magnetic moments of these clusters are $8 \mu_B$. Cr_4Te_6 is a tetrahedral structure with a core of Cr_4 with each Cr-Cr bond decorated by a Te atom. The cluster has no net spin and the local spin moments at the Cr sites are also quenched. The magnetic property of this particular cluster has been studied in detail further.

The ground state of Cr_5 cluster is a distorted triangular bipyramidal structure with net moment of $6 \mu_B$ and a ferrimagnetic spin configuration. With the addition of Te atoms, the net spin magnetic moment fluctuates. With the addition of 1, 2, 3 and 4 Te, the clusters are ferrimagnetic with three spin up and two spins down local moments on Cr sites. For Cr_5Te_5 and Cr_5Te_6 clusters, high spin magnetic moment of $10 \mu_B$ is seen due to their ferrimagnetic configuration of four up and one down states among chromium atoms. With seven Te atoms, the high magnetic moment is quenched to $2 \mu_B$ with 3 up and 2 down antiferromagnetic state.

The Cr_6Te_n series is particularly interesting due to the high symmetry of Cr_6 core. Bare Cr_6 clusters are antiferromagnetically aligned moments with no net spin. Addition of 1, 2, 3 and 4 Te atoms to bare Cr_6 clusters doesn't affect the net magnetic moment. The six chromium atoms are still antiferromagnetically aligned with net spin zero. The average Cr-Cr bond distance is stretched from 2.38 \AA in bare Cr_6 clusters to 2.69 \AA , 2.69 \AA and 2.67 \AA respectively for the next three clusters in series. With addition of 5, 6, 7 and 8 Te atoms, the net magnetic spin increases and are ferrimagnetically aligned resulting in a moment of $6 \mu_B$, $4 \mu_B$, $6 \mu_B$, and $6 \mu_B$ respectively. Cr_6Te_8 cluster is highly symmetric with a net moment of $6 \mu_B$. The core comprises of a distorted octahedron with each face decorated by a Te atom. The symmetry point group of the cluster is D_{2d} . The magnetic spins are ferrimagnetic and the geometry is same as found in ligated Cr_6Te_8 clusters. Ligated

Cr_6Te_8 clusters has been synthesized in solution by Hessen et al¹⁶. From Fig 6 , it can be concluded that the largest moment is attained for Cr_5Te_5 and Cr_5Te_6 clusters. Three clusters, Cr_2Te_3 , Cr_2Te_4 and Cr_4Te_6 are seen to be non-magnetic with all local Cr spin magnetic moments quenched.



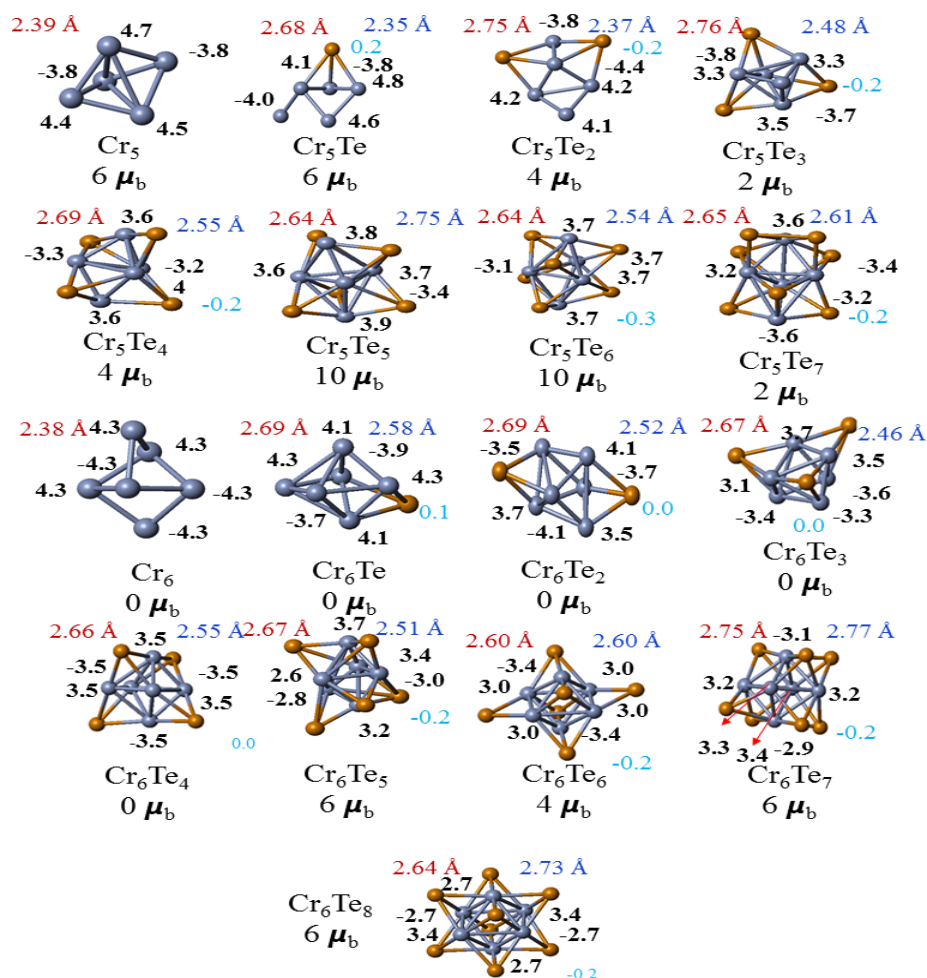


Figure 5 : Structure, Magnetic spin and average bond distances of Cr_nTe_m clusters ($n = 1 - 6$, $m = 1 - 8$)

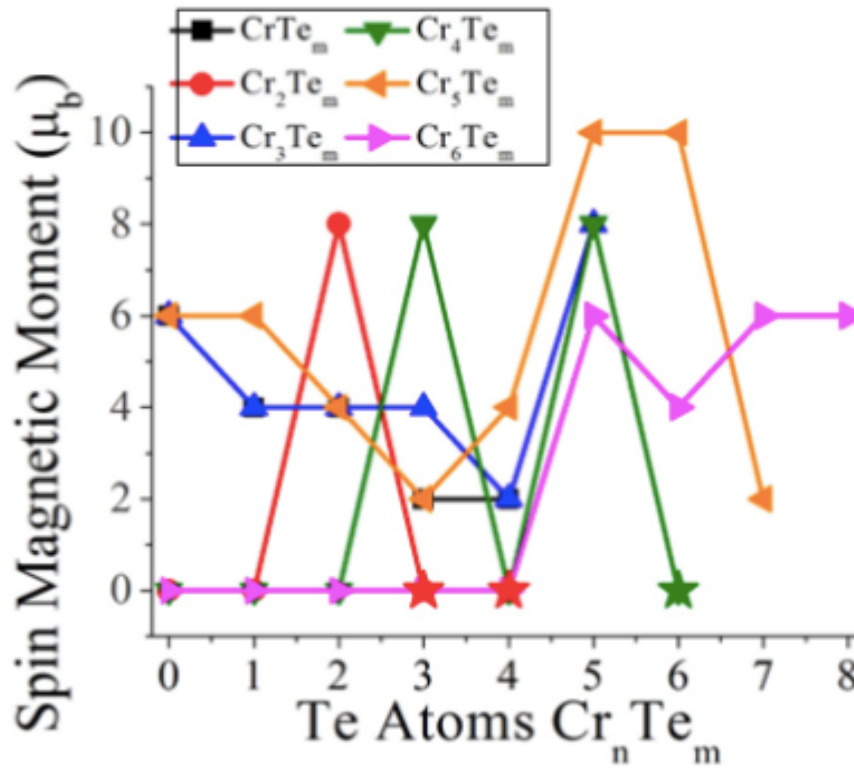


Figure 6 : Spin Magnetic Moment (μ_b) of $Cr_n Te_m$ clusters ($n = 1 - 6$, $m = 1 - 8$)

3.3 HOMO-LUMO Gaps of Cr_nTe_m Clusters

HOMO-LUMO gap exhibits the electronic stability of a cluster. Higher HOMO-LUMO gap of a cluster indicates its low reactivity and enhanced electronic stability. Figure 7 shows the change in HOMO-LUMO gap within the Cr_nTe_m series ($n=1-6$, $m=0-8$). For CrTe_m ($m=0-4$) clusters, there is a drop in HOMO-LUMO gap with addition of Te atoms as a result of which they have a net magnetic moment due to unpaired electrons. Cr atom and Cr_2 dimer have large HOMO-LUMO gap, however they have local spin moments. As seen for CrTe_m , the HOMO-LUMO gaps in Cr_2Te_m also decreases with addition of Te atoms. However, Cr_2Te_4 cluster has unusually high HOMO-LUMO gap of 1.51 eV which also marks its high electronic stability and reduced reactivity. Another prominent change in HOMO-LUMO gap is seen for Cr_4Te_6 cluster which has a high gap of 1.40 eV making it one of the most stable cluster. The remaining clusters have relatively low HOMO-LUMO gaps (less than 1 eV) and most have gaps less than 0.5 eV.

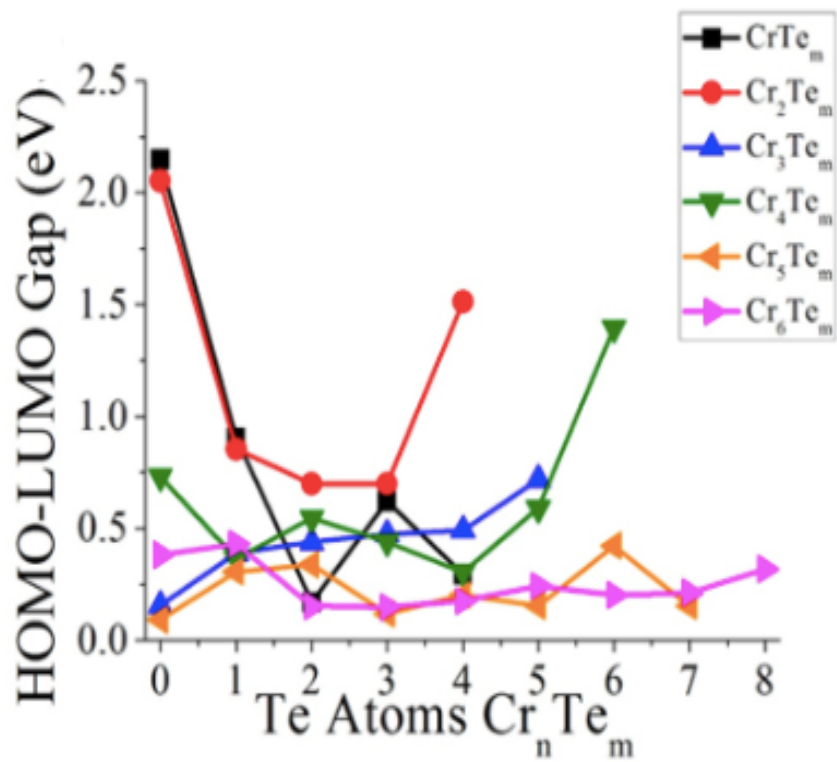


Figure 7 : HOMO - LUMO gaps of $Cr_n Te_m$ clusters ($n = 1 - 6$, $m = 1 - 8$)

3.4 Fragmentation and Binding Energies of $Cr_n Te_m$ Clusters

Fragmentation Energy (F.E) of a cluster is the indication of its energetic stability. The higher the fragmentation energy, the more stable is the cluster. Fig 8 shows the fragmentation energies of all the clusters examined in this study. The fragmentation energy increases with addition of Te atoms for most of the clusters. We analyzed the energetics of all the fragmentation channels using Eq. 1, for all possible x and y.

$$F.E. = E(Cr_x Te_y) + E(Cr_{n-x} Te_{m-y}) - E(Cr_n Te_m) \quad (1)$$

This represents the energy required to break a $Cr_n Te_m$ cluster into fragments containing $Cr_x Te_y$ and $Cr_{n-x} Te_{m-y}$ atoms. We then identified the lowest fragmentation energy channel for all clusters studied here. The largest fragmentation energies are for $Cr_6 Te_8$, and $Cr_4 Te_6$, with the fragmentation channel being the removal of Te in both cases. $Cr_4 Te_6$ is found to be highly stable both energetically and electronically. $Cr_6 Te_8$ is found to be highly stable to fragmentation but has a small HOMO-LUMO gap of 0.32 eV. In general, the fragmentation energy increases with the number of Te atoms, and for clusters with a large proportion of Te, Te removal is the most likely fragmentation channel. For clusters with more Cr than Te, the Cr removal is consistently the lowest energy fragmentation channel.

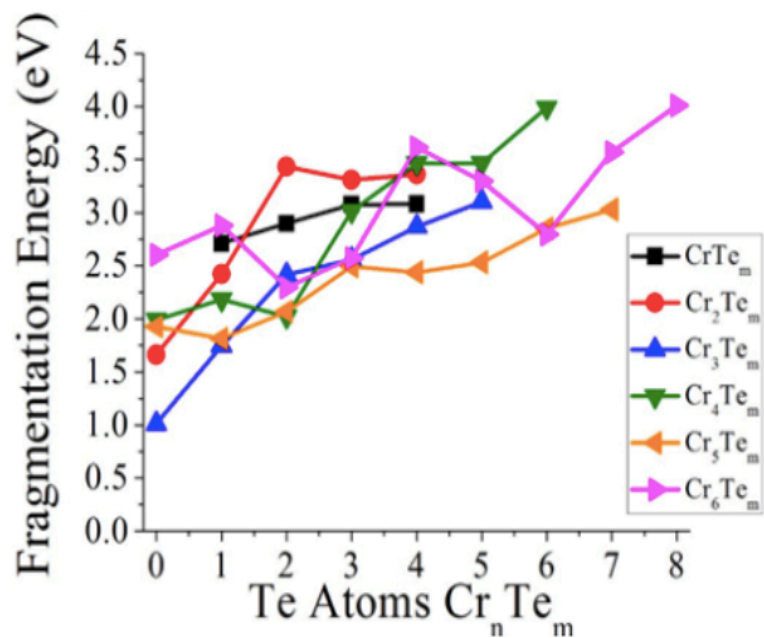


Figure 8 : Fragmentation Energies of $Cr_n Te_m$ clusters ($n = 1 - 6$, $m = 1 - 8$)

3.5 Ionization Potentials & Electron Affinities of $\text{Cr}_n \text{Te}_m$ Clusters

Fig 9 A) and B) shows the adiabatic Ionization energy and adiabatic Electron affinities of $\text{Cr}_n \text{Te}_m$ clusters. Ionization energies generally increases with the addition of Te atoms with CrTe_m and $\text{Cr}_2 \text{Te}_m$ towards the higher realm. The increase in Ionization energy with addition of Te atoms is due to electron acceptor characteristic of tellurium. $\text{Cr}_2 \text{Te}_3$ and $\text{Cr}_2 \text{Te}_4$ have quite high Ionization energies of 7.36 eV and 7.38 eV respectively. $\text{Cr}_3 \text{Te}_m$ shows a steep rise in IP with addition of Te atoms up to four Te atoms and the IP drops from $\text{Cr}_3 \text{Te}_4$ to $\text{Cr}_3 \text{Te}_5$. The IP of $\text{Cr}_n \text{Te}_m$ ($n=4,5,6$) clusters increases with addition of Te atoms. $\text{Cr}_4 \text{Te}_6$ cluster has a high Ionization energy of 7.34 eV. This is consistent with clusters having closed electronic shell. $\text{Cr}_6 \text{Te}_8$ has a lower Ionization energy consistent with clusters with open electronic shells. It is seen that all of the non-magnetic clusters have high ionization energies making them relatively less electron donors.

Figure 9 B) shows the adiabatic electron affinities of $\text{Cr}_n \text{Te}_m$ clusters. Tellurium atom is a good electron acceptor and so addition of Te atoms increases the overall electron affinity of the clusters. There is a general trend in increase of electron affinity with systematic addition of Te atoms among all the bare chromium clusters. Notably, $\text{Cr}_4 \text{Te}_6$ has a relatively large electron affinity of 2.76 eV. This number is quite high for a cluster with closed electronic shell. On the other hand, $\text{Cr}_6 \text{Te}_8$ has the highest electron affinity among all the studied clusters which may be due to its electronic open shell structure. Other notably large electron affinities include the $\text{Cr}_5 \text{Te}_5$, $\text{Cr}_6 \text{Te}_5$ and $\text{Cr}_6 \text{Te}_7$ clusters, which have electron affinities of 3.09 eV, 3.15 eV, and 3.21 eV, respectively. This shows that $\text{Cr}_6 \text{Te}_8$ cluster could bind charge donating ligand strongly as the cluster is a strong electron

acceptor. Binding will be enhanced when the ligand is an electron donor. It has been observed²⁵⁻²⁷ that $\text{Cr}_6\text{Te}_8(\text{PET}_3)_6$ is very stable as a result of chemical stability obtained as the donor ligands such as PET_3 are added to the cluster.

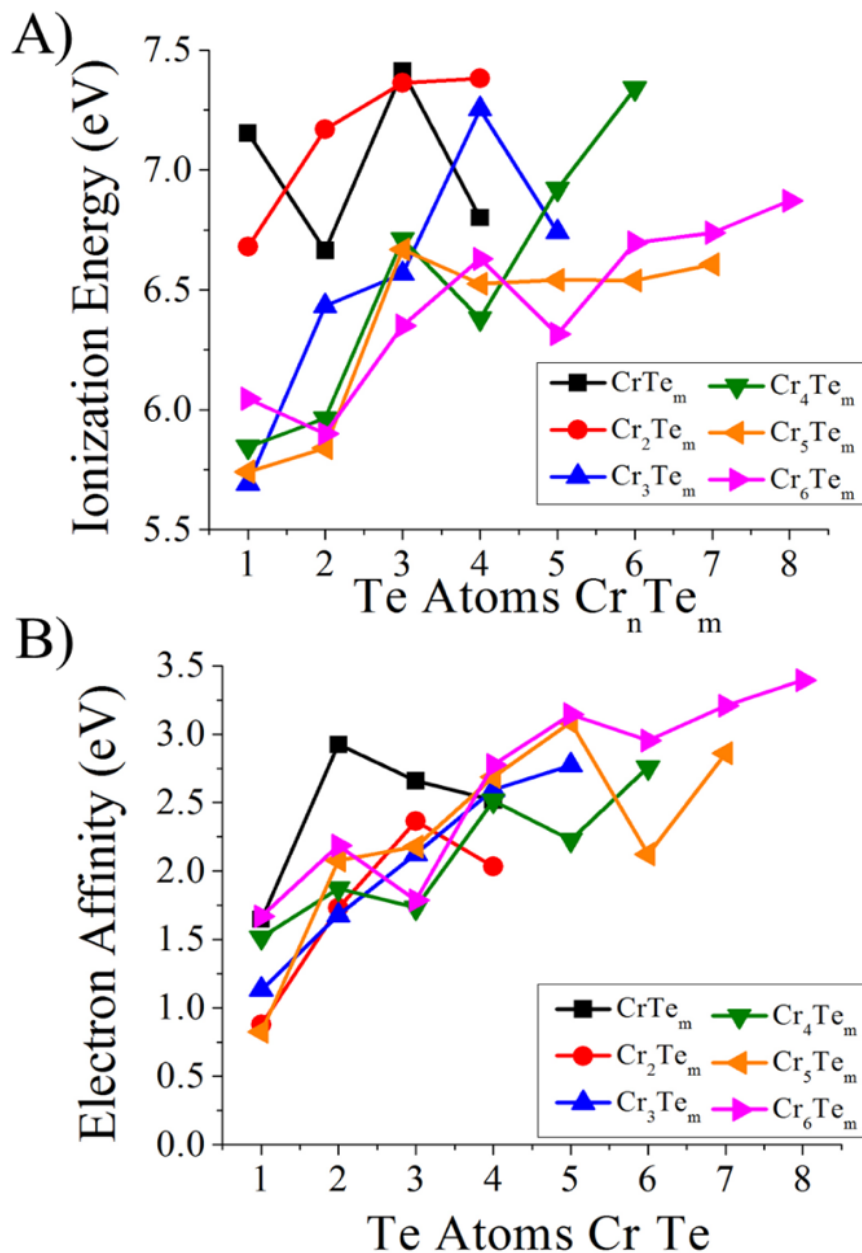


Figure 9 : A. Ionization Energies of Cr_nTe_m clusters ($n = 1 - 6$, $m = 1 - 8$)
 B. Electron Affinities of Cr_nTe_m clusters ($n = 1 - 6$, $m = 1 - 8$)

3.6 3d-orbital Occupation of Cr_n Te_m Clusters

Figure 10 shows the 3d occupation of chromium starting from bare chromium atom which has half-filled 3d shell. The d-orbital occupation reduces in up channel and increases in the down channel while binding with tellurium atoms.

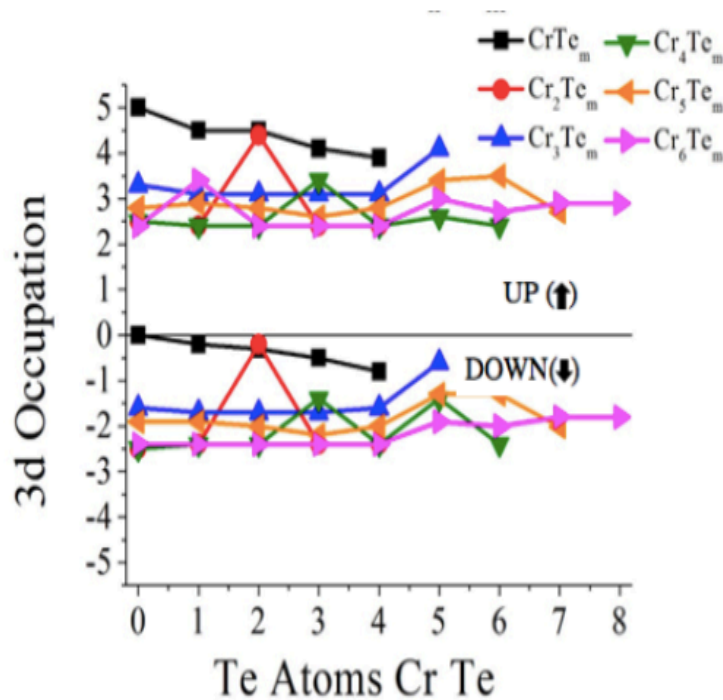


Figure 10 : 3 d Occupation of Cr atoms in the up and down channel of Cr_n Te_m clusters (n = 1 - 6, m = 1 - 8)

IV. Stable Clusters: Cr_4Te_6 and Cr_6Te_8

From the above examinations, two clusters were found to be particularly stable. Cr_4Te_6 cluster is non-magnetic with a large HOMO-LUMO gap of 1.4 eV which accounts for its electronic stability. Along with large HOMO-LUMO gap, it also has a high value of fragmentation energy (4.0 eV). Both these properties make this cluster very stable both electronically and chemically. The non-magnetic state with no local spins on Cr sites is assumed to be the result of high HOMO-LUMO gap. We further study the electronic states of Cr_4Te_6 by analyzing the 3d orbital splitting of bare chromium atom after addition of tellurium atoms.

Cr_6Te_8 cluster is energetically stable evident from its high fragmentation energy. However, Cr_6Te_8 has lower value of HOMO-LUMO gap. The net moment of the cluster is zero, but the chromium sites have local moments due to unpaired spins present in chromium atoms. This cluster is particularly interesting because of its high electron affinity coupled with energetic stability that binds the clusters with electron donating ligands like PET_3 . $\text{Cr}_6\text{Te}_8(\text{PET}_3)_6$ cluster has been vastly synthesized and studied²⁵⁻²⁷. The ligated clusters can be optimized to form Cluster Assembled Materials. For example, ligated $\text{Cr}_6\text{Te}_8(\text{PET}_3)_6$ clusters caps C_{60} to form building blocks of CAMs.

Both these clusters have been intensively studied through ADF set of codes. The orbital occupation was analyzed that gave us a brief idea of the type of splitting taking place due to the effect of Te atoms.

4.1 Electronic and Chemical Properties of Cr_4Te_6 Clusters

Cr_4Te_6 clusters is chemically very stable pertaining to its high value for fragmentation energy. It is highly symmetric with a tetrahedral symmetry (T_d). Due to the symmetry, all chromium atoms are considered equivalent. This cluster is non-magnetic with no local spins and has a large HOMO-LUMO gap. The large HOMO-LUMO gap marks its high electronic stability and low reactivity. Both its electronic and chemical stability makes it an interesting candidate for study. The orbital structure of chromium atom in the cluster is investigated. The 3d-orbital splitting is studied by comparing the bare chromium 3d-orbitals with the 3d-orbitals of the chromium from the cluster. The large HOMO-LUMO gap of 1.40 eV implies that the Cr atoms undergoes a significant ligand field splitting.

4.2 d-Orbital Splitting of Cr in Cr_4Te_6 Clusters

Figure 11 shows the ligand field splitting of Cr_4Te_6 . As the cluster had T_d symmetry, all Cr atoms are equivalent. The lowest energy 3d orbital is the $3d_z^2$ bonding orbital where all four Cr atoms form a bonding orbital. Next, and close in energy is the bonding orbitals between Cr $3d_{xy}/3d_{x^2-y^2}$ and Te. A set of weaker bonding Cr $3d_{xz}$ and $3d_{yz}$ orbitals then make up the HOMO of the cluster. The LUMO is then a weak $3d_{z^2}$ antibonding orbital, where the antibonding is between the Cr atoms, so the shift in energy is small. Next, the antibonding Cr $3d_{xy}/3d_{x^2-y^2}$ and Cr $3d_{xz}3d_{yz}$ orbitals make up the rest of the 3d shell. It is interesting to note that the deepest bonding orbital is the $3d_{z^2}$, orbitals with other Cr, and not with Te, and that the tetrahedral structure leads to the Cr $3d_{xy}/3d_{x^2-y^2}$ orbitals to be degenerate. The high symmetry and ligand field splitting explains the large electronic stability of Cr_4Te_6 .

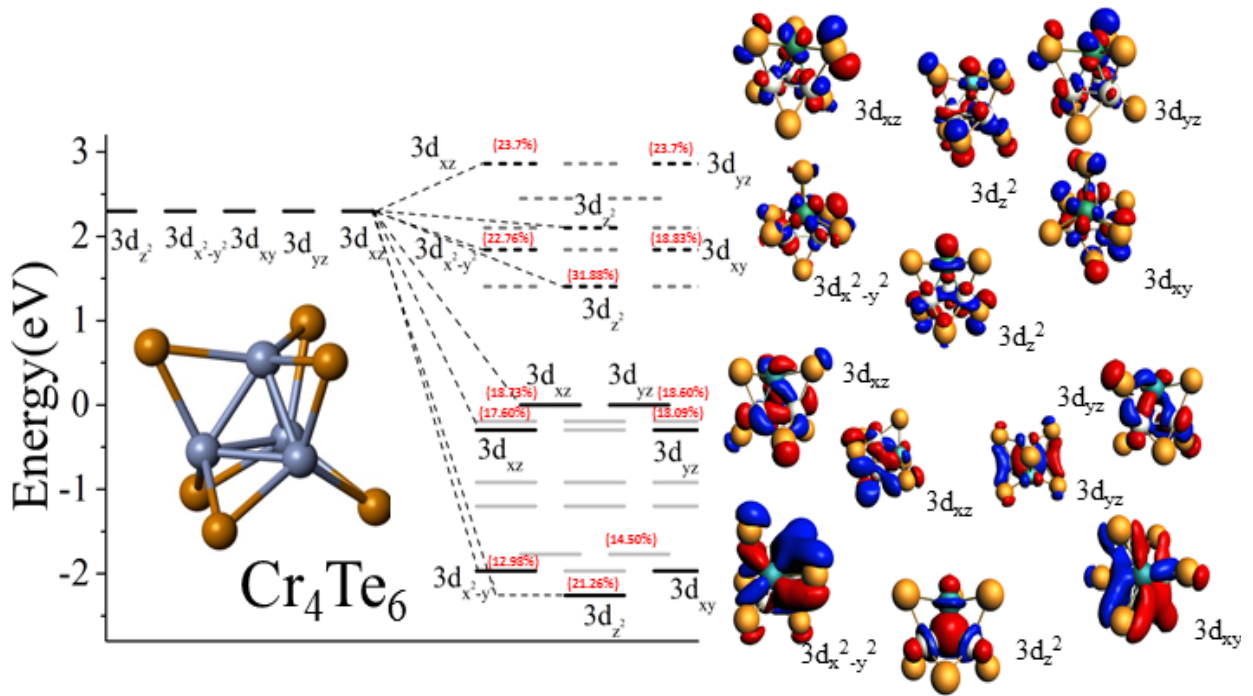


Figure 11 : The ligand field splitting of Cr₄ Te₆. The red percentages give the percent of the orbital corresponding to the Cr 3 d orbital

4.3 Electronic and Chemical Properties of Cr_6Te_8 Clusters

Another cluster of interest is Cr_6Te_8 cluster. The high electron affinity and chemical stability makes it an interesting cluster. Owing to its ability to accept electron, a good amount of research ²⁵⁻²⁷ has been performed to synthesize ligated Cr_6Te_8 clusters which forms the building blocks for CAMs. Understanding the orbital properties of the non-ligated cluster give us an outlook about the nature of electronic states in the bare cluster and we can better understand the bonding type with ligands. The cluster has a symmetry of D_{2d} with three inequivalent chromium atoms.

4.4 d-Orbital Splitting of Cr in Cr₆ Te₈ Clusters

The orbital splitting is shown in Figure S1-S3, where orbitals with significant 3d occupation are shown. The lowest energy 3d orbital in all cases is the $3d_{xy}$ orbital which bonds strongly with the 4 surrounding Te atoms. Next is the $3d_{z^2}$ orbital that bonds with the Cr atom on the opposite side of the cluster. The $3d_{xz}$ and $3d_{yz}$ orbitals are next in increasing energy, followed by the mostly non-bonding $3d_{x^2-y^2}$ orbital. The last filled orbital in the spin majority channel is the $3d_{z^2}$ orbital which is antibonding with the Cr atom on the opposite side of the cluster. The next unfilled orbitals in the Cr atom is the $3d_{z^2}$ antibonding orbital, and the $3d_{xy}$ antibonding orbital. The ordering is quite different from that in Cr₄ Te₆, with the degeneracy between $3d_{xy}$ and $3d_{x^2-y^2}$ found in Cr₄ Te₆ being broken as the bonding with Te moves from three-fold to four-fold. While other Cr sites have different electronic structures, the ordering of the orbitals is essentially the same. We also note that the exchange splitting is reasonably large, 1-2 eV, so the local spin magnetic moments are still present.

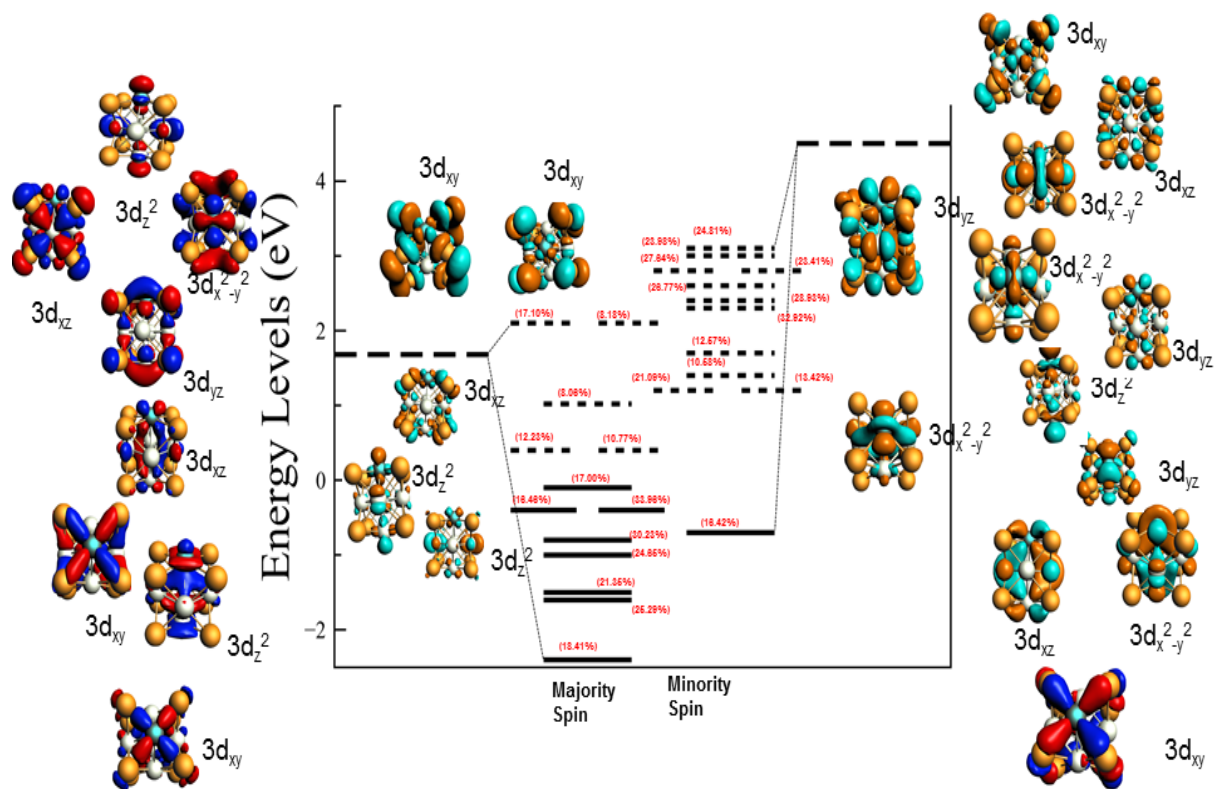


Figure S2 : The ligand field splitting of two Cr atoms in Cr_6Te_8 . The red percentages give the percent of the orbital corresponding to the Cr 3d orbital.

Red and blue orbitals are filled, and cyan and orange orbitals are empty

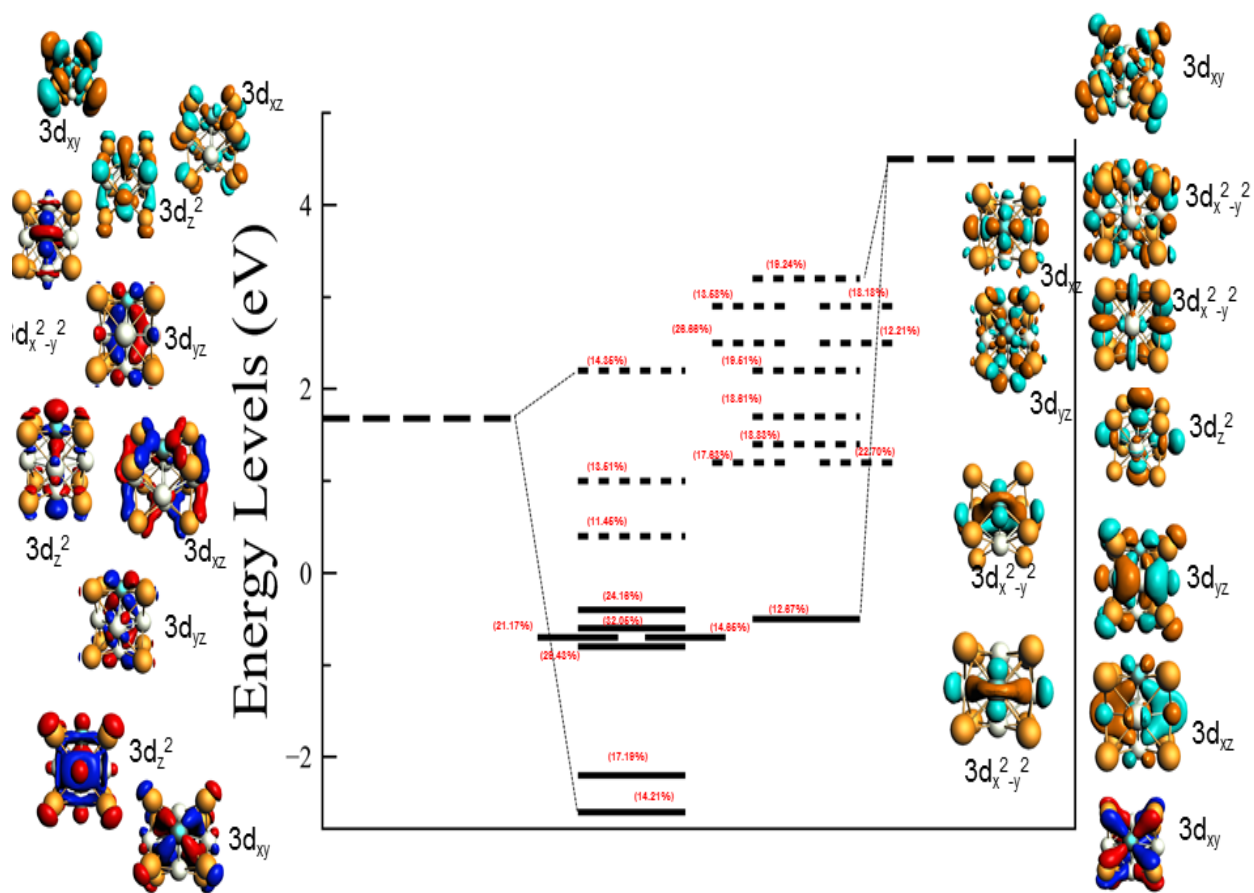


Figure S3 : The ligand field splitting of two Cr atoms in Cr_6Te_8 . The red percentages give the percent of the orbital corresponding to the Cr 3d orbital. Red and blue orbitals are filled, and cyan and orange orbitals are empty

To investigate if the addition of ligands can further stabilize the cluster, electronic structure calculation was carried out on $\text{Cr}_6\text{Te}_8(\text{PEt}_3)_6$ cluster where six charge donating PEt_3 ligands were added to the Cr sites. The structure was optimized without any constraint and various spin states and the couplings were investigated. We found that the addition of ligands increased the HOMO-LUMO gap to 0.78 eV indicating an electronically stable cluster. Further the Cr sites were antiferromagnetically coupled with an overall moment of $0 \mu_B$. The Cr sites carry local moments ranging from -3.1 to

3.1 μ_B . The presence of local moments is consistent with the magnetic data that indicates Cr sites couple antiferromagnetically²⁸. The bond distances are also consistent with the X-ray structure of the clusters. Experimentally, there is some discrepancy over the experimental spin magnetic moment, with Kamiguchi et al.²⁹ reporting that the cluster is antiferromagnetic, while Steigerwald et al. found that the effective moment was 2.8 μ_B ²⁸. We suspect that the higher moment is due to the ionized clusters having a larger spin magnetic moment, although orbital spin may also play a role.

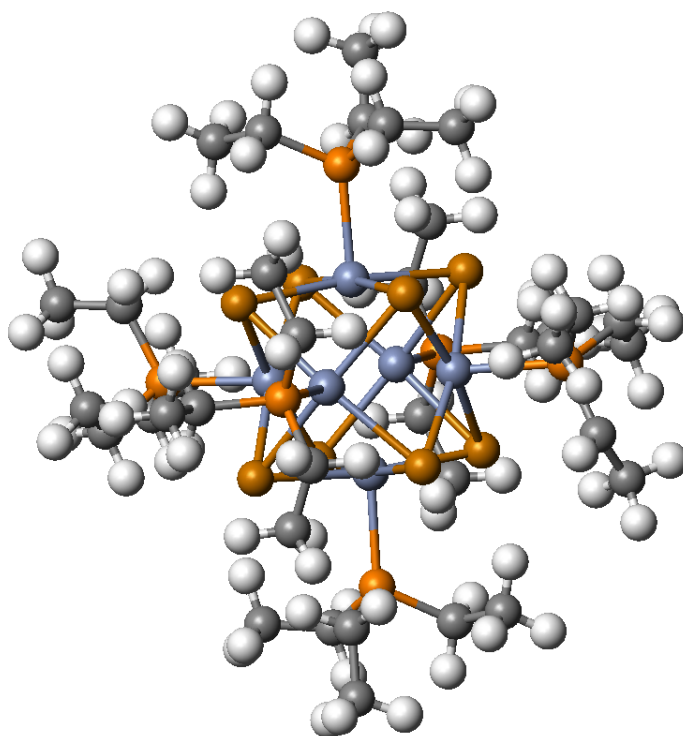


Figure 12 : The structure, spin magnetic moment, ionization energy and electron affinity of $\text{Cr}_6\text{Te}_8(\text{PEt}_3)_6$

V. DISCUSSION & CONCLUSION

In the present work, metal chalcogenide chromium tellurium clusters have been investigated through First principle electronic structure studies using Amsterdam Density Functional (ADF) set of codes. The study has been divided into four parts. Firstly, pure chromium clusters are studied from sizes ranging from one chromium atom to six chromium atoms. The second part deals with the effect of addition of chalcogenide Tellurium. Two clusters (Cr_4Te_6 and Cr_6Te_8) seemed to be particularly interesting owing to their high electronic and chemical stability. The detailed orbital structure of these two clusters are presented in the third part. The fourth section is the extension of electronic property of Cr_6Te_8 cluster where we talk about effect of adding ligands to this cluster.

Pure chromium atom has an atomic number of 24 and has a ground state of 7S_3 in a $3d^54s^1$ configuration. Due to its six unpaired electrons in d and s orbitals, it exhibits a net magnetic moment of $6 \mu_B$. Chromium forms an antiferromagnetically paired chromium dimer with a bond length of 1.68 \AA which is much lower than Cr-Cr distance in bulk chromium metal which is 2.50 \AA with a body centered cubic ¹³ structure. This is one of the examples that distinguish a cluster from its bulk in terms of its properties. The binding energy of chromium dimer is too low as a result of size difference between 4s and 3d orbital as well as effect of exchange energy which prevents it from forming six bonds. The bond length increases with addition of more chromium atoms. Also, the net magnetic moment changes which has been shown in the first section of this thesis. All the pure chromium clusters have local magnetic moments at the Cr sites.

With the addition of Te atoms to the pure chromium cluster, the geometry as well as magnetic properties changes. For CrTe_m series, the net moment of chromium atom is quenched from $6 \mu_B$ to 4

μ_B with addition of 1, 2 and 3 Te atoms. The moment becomes $2 \mu_B$ with 4 Te atoms. For $Cr_2 Te_m$ clusters, the bond length increases with addition of Te atoms. With addition of two Te atoms, the cluster becomes ferromagnetic due to super-exchange interaction. However, with further addition of Te atoms, the local spins are all quenched leaving $Cr_2 Te_3$ and $Cr_2 Te_4$ nonmagnetic. Cr_3 cluster has a net magnetic moment of $6 \mu_B$. The moment is quenched up to addition of 4 Tellurium atoms, but the structure become more symmetric with Te bridging in $Cr_3 Te_5$ as a result of which the cluster is ferromagnetic. Cr_4 cluster is not equivalent to two Chromium dimers as the bond length of Cr_4 is greater than Cr_2 . Chromium tetramer is antiferromagnetic and with addition of Te atoms, the bond length is stretched. Addition of three Te atoms makes it magnetic with three up spin and one down spin chromium atoms. $Cr_4 Te_4$ is antiferromagnetic and $Cr_4 Te_5$ is ferrimagnetic. With addition of six Te atoms, the local spins on Cr sites are completely quenched resulting in a non-magnetic stable cluster with high HOMO-LUMO gap and large fragmentation energy. The $Cr_5 Te_m$ series is mostly magnetic with majority up spin chromium atoms.

In $Cr_6 Te_m$ clusters, Cr sites are antiferromagnetically coupled up to $m=4$. The net magnetic moment increases with addition of more Te atoms. $Cr_6 Te_8$ is particularly interesting due to its high value of fragmentation energy marking its energetic stability but high electron affinity. This leads to its property of binding with charge donating ligands to form cluster assembled materials.

Properties of two clusters are discussed in detail due to their high stability. $Cr_4 Te_6$ cluster stand out for its electronic as well as chemical stability. It is found that $Cr_4 Te_6$ cluster is non-magnetic with no local spin on chromium sites. It also has a large value of HOMO-LUMO gap of 1.40 eV which makes it electronically stable. Along with electronic stability, it is also energetically stable evident from the high value of fragmentation energy. The orbital structure of this cluster was further

studied. It is found that there is a ligand field splitting of 3d orbitals of Cr in Cr_4Te_6 cluster. The cluster has a tetrahedral symmetry and all the Cr atoms are equivalent. The lowest energy bonding orbital is $3d_{z^2}$ where all the four Cr atoms form bonding orbital. Next is the bonding orbital between the Cr $3d_{xy}/3d_{x^2-y^2}$ and Te. This is followed by a couple of weaker bonding $3d_{xz}$ and $3d_{yz}$ orbitals which also makes up the HOMO. The LUMO is a weak antibonding orbital where the antibonding is between the Cr atoms. Next the antibonding Cr $3d_{xy}/3d_{x^2-y^2}$ and Cr $3d_{xz}/3d_{yz}$ orbitals make up the rest of the 3d shell. The deepest bonding orbitals are between Cr and not with Te. There is degeneracy seen due to the symmetric tetrahedral structure. $3d_{xy}$ and $3d_{x^2-y^2}$ are degenerate, also $3d_{xz}$ and $3d_{yz}$ are degenerate. The high electronic stability is explained by high symmetry and ligand field splitting.

Next, the electronic structure of Cr_6Te_8 cluster has been evaluated. This cluster displays a very high value of fragmentation energy, hence very stable energetically and its high electron affinity enables it to bind with electron donating ligands which has been briefly introduced. The cluster has D_{2d} symmetry so there are three inequivalent Cr atoms. The orbital splitting diagrams of all these three atoms has been analyzed. $3d_{xy}$ is the lowest energy 3d orbital in all the cases which bonds strongly with Te atoms unlike Cr_4Te_6 cluster in which Cr-Cr form the lowest bonding orbital. Next is $3d_{z^2}$ orbital that bonds Cr atoms in the opposite side of the cluster followed by slightly bonding degenerate orbitals $3d_{xz}$ and $3d_{yz}$ orbitals. The next in energy is the non-bonding $3d_{x^2-y^2}$ orbital. The last filled orbital in spin majority channel is $3d_{z^2}$ which is non-bonding with Te and weakly bonding with adjacent Cr but antibonding with opposite Cr. The unfilled orbitals are non-bonding with Te and antibonding with Cr $3d_{z^2}$ orbital. There is no degeneracy seen due to symme-

try as was visualized for Cr_4Te_6 cluster. Local spin magnetic moments are still present due to large value of exchange splitting.

Finally the structure and properties of Cr_6Te_8 cluster were examined with addition of six electron donating PEt_3 ligands. The ligands were attached to the six chromium sites. It is found that HOMO-LUMO gap increases with addition of ligands which is an indication of enhanced stability of the ligated cluster. The Cr sites were antiferromagnetically coupled with overall spin $0 \mu_B$. The available magnetic data matches the calculated local moment of Cr sites.

VI. SUMMARY & FUTURE DIRECTIONS

The structure, stability, spin magnetic ground states, and electronic properties of metal chalcogenide Cr_nTe_m clusters, $n=1-6$, $m=0-8$ has been investigated. It is found that pure chromium clusters show completely different physical, chemical and magnetic properties from its bulk and addition of Te atoms to bare chromium cluster affects the bond length, magnetic spins and HOMO-LUMO gaps of the cluster. The electronic and orbital properties of a cluster can also be studied to understand their bonding capacity to form ligated clusters. Cr_4Te_6 and Cr_6Te_8 clusters are found to be particularly stable. Cr_4Te_6 has nonmagnetic ground state spin with no local moments on chromium atoms. It also displays high HOMO-LUMO gap which is a marker of its electronic stability. The origin of the magnetic quenching in Cr_4Te_6 cluster is assumed to be through ligand field splitting of Cr 3d-orbitals. Cr_6Te_8 is energetically stable due to its symmetric structure and a greater number of Cr-Te bonds. This cluster has extremely high electron affinity of 3.39 eV and has open electronic shell due to which it readily bonds with electron donating ligands. This explains the high stability of $\text{Cr}_6\text{Te}_8(\text{PEt}_3)_6$. The ground state structure of $\text{Cr}_6\text{Te}_8(\text{PEt}_3)_6$ cluster is antiferromagnetic and ligated cluster has a much lower ionization energy and electron affinity as compared to ligated clusters.

This study opens the scope for analyzing more ligated clusters and observe the behavior of the clusters on adding different type of ligands. The superexchange mechanism of Te bridging two Cr atoms can also be researched in detail. The information and data collected during the study can be utilized to predict the properties and characteristics of other ligated and non-ligated clusters.

VII. BIBLIOGRAPHY & REFERENCES

- ¹A. Pinkard, A.M. Champsaur, and X. Roy, *Acc. Chem. Res.* **51**, 919 (2018).
- ²X. Roy, C.-H. Lee, A.C. Crowther, C.L. Schenck, T. Besara, R.A. Lalancette, T. Siegrist, P.W. Stephens, L.E. Brus, P. Kim, M.L. Steigerwald, and C. Nuckolls, *Science* **341**, 157 (2013).
- ³Herzing, A. A.; Kiely, C. J.; Carley, A. F.; Landon, P.; Hutchings, G. J. Identification of Active Gold Nanoclusters on Iron Oxide Supports for CO Oxidation. *Science* **321**, 5894 (2008).
- ⁴Knight W D, Clemenger K, de Heer W A, Saunders W A, Chou M Y and Cohen M L *Phys. Rev. Lett.* **52**, 2141 (1984).
- ⁵Xi Li, Hongbin Wu, Xue-Bin Wang, and Lai-Sheng Wang *Phys. Rev. Lett.* **81**, 1909 (1998).
- ⁶A. W. Castleman, S. N. Khanna, "Clusters, Superatoms, and Building Blocks of New Materials", *J. Phys. Chem.*, **113**, 2664 (2009)
- ⁷S. A. Claridge, A. W. Castleman, S. N. Khanna, C. B. Murray, A. Sen, P. S. Weiss, "Cluster-Assembled Materials", *ACS NANO*, **3**, 244 (2009)
- ⁸Song Jin, Friedrich Popp, Shannon W. Boettcher, Min Yuan, Catherine M. Oertel, Francis J. DiSalvo "Synthesis, characterization and properties of Mo₆S₈(4-tert-butylpyridine)₆ and related M₆S₈L₆ cluster complexes (M = Mo, W)", *J. Chem. Soc., Dalton Trans.* **16** 3096 (2002)
- ⁹Vikas Chauhan, Sanjubala Sahoo, and Shiv N. Khanna "Ni₉Te₆(PEt₃)₈C₆₀ Is a Superatomic Superalkali Superparamagnetic Cluster Assembled Material (S3-CAM)" *J. Am. Chem. Soc.*, **138(6)** 1916 (2016)
- ¹⁰H.J Zhai, L S Wang, "Probing the electronic properties of dichromium oxide clusters Cr₂O_n- (n=1-7) using photoelectron spectroscopy" *J.Chem.Phys.* **125** 164315 (2006)
- ¹¹G. te Velde, F.M. Bickelhaupt, E.J. Baerends, C. Fonseca Guerra, S.J.A. van Gisbergen, J.G. Snijders, and T. Ziegler, *J. Comput. Chem.* **22**, 931 (2001).
- ¹²J.P. Perdew, K. Burke, and M. Ernzerhof, *Phys. Rev. Lett.* **77**, 3865 (1996).
- ¹³E. van Lenthe, J.G. Snijders, and E.J. Baerends, *J. Chem. Phys.* **105**, 6505 (1996).
- ¹⁴B Delley, AJ Freeman, DE Ellis, *Phy. Rev. Lett.* **50**, 488 (1983).
- ¹⁵D.L. Michalopoulos, M.E. Geusic, S.G. Hansen, D.E. Powers, and R.E. Smalley, *J. Phys. Chem.* **86**, 3914 (1982).
- ¹⁶C.X. Su, D.A. Hales, and P.B. Armentrout, *Chem. Phys. Lett.* **201**, 199 (1993).
- ¹⁷K. Hilpert and R. Ruthardt, *Berichte Bunsenges. Für Phys. Chem.* **91**, 724 (1987).
- ¹⁸C. -X. Su and P.B. Armentrout, *J. Chem. Phys.* **99**, 6506 (1993).
- ¹⁹H.-J. Zhai and L.-S. Wang, *J. Chem. Phys.* **125**, 164315 (2006).
- ²⁰L.-S. Wang, H. Wu, and H. Cheng, *Phys. Rev. B* **55**, 12884 (1997). Hirsch, K.; Zamudio-Bayer, V.;
- ²¹Ameseder, F.; Langenberg, A.; Rittmann, J.; Vogel, M.; Möller, T.; v. Issendorff, B.; Lau, J. T. 2p x-ray absorption of free transition-metal cations across the 3d transition elements: Calcium through copper. *Phys. Rev. A* **2012**, 85 (6)
- ²²Cheng, H.; Wang, L.-S. Dimer growth, structural transition, and antiferromagnetic ordering of small chromium clusters. *Phys. Rev. Lett.* **1996**, 77 (1), 51.

- ²³Baykara, N. A.; McMaster, B. N.; Salahub, D. R. LCAO local-spin-density and $X\alpha$ calculations for Cr_2 and Mo_2 . *Mol. Phys.* **1984**, 52 (4), 891-905
- ²⁴Loópez-Estrada, O.; Loópez-Olay, S.; Aburto, A.; Orgaz, E. Unexpected High Spin Polarization in Cr_4 Cluster. *J. Phys. Chem. C* **2016**, 120 (41), 23892-23897
- ²⁵H. Metiu, S. Chrétien, Z. Hu, B. Li, and X. Sun, *J. Phys. Chem. C* **116**, 10439 (2012).
- ²⁶Y. Yang, A.C. Reber, S.E. Gilliland, C.E. Castano, B.F. Gupton, and S.N. Khanna, *J. Catal.* **360**, 20 (2018).
- ²⁷Y. Yang, A.C. Reber, S.E. Gilliland, C.E. Castano, B.F. Gupton, and S.N. Khanna, *J. Phys. Chem. C*, **122**, 25396 (2018).
- ²⁸B. Hessen, T. Siegrist, T. Palstra, S.M. Tazler, and M.L. Steigerwald, *Inorg. Chem.* **32**, 5165 (1993).
- ²⁹S. Kamiguchi, H. Imoto, T. Saito, and T. Chihara, *Inorg. Chem.* **37**, 6852 (1998).
- ³⁰J. Yu, C.-H. Lee, D. Bouilly, M. Han, P. Kim, M.L. Steigerwald, X. Roy, and C. Nuckolls, *Nano Lett.* **16**, 3385 (2016).
- ³¹V. Chauhan, A. C. Reber, and S. N. Khanna, *Phys. Chem. Chem. Phys.* **19**, 31940 (2017).
- ³²A.C. Reber and S.N. Khanna, *Acc. Chem. Res.* **50**, 255 (2017).
- ³³E.S. O'Brien, M.T. Trinh, R.L. Kann, J. Chen, G.A. Elbaz, A. Masurkar, T.L. Atallah, M.V. Paley, N. Patel, D.W. Paley, I. Kymissis, A.C. Crowther, A.J. Millis, D.R. Reichman, X.-Y. Zhu, and X. Roy, *Nat. Chem.* **9**, 1170 (2017).
- ³⁴V. Chauhan, A.C. Reber, and S.N. Khanna, *J. Am. Chem. Soc.* **139**, 1871 (2017).
- ³⁵S.N. Khanna and A.C. Reber, *Nat. Chem.* **9**, 1151 (2017).
- ³⁶H. Brunner, H. Catey, W. Meier, Y. Mugnier, A.C. Stückl, J. Wachter, R. Wanninger, and M. Zabel, *Chem. - Eur. J.* **9**, 3796 (2003).
- ³⁷T.T.M. Palstra, M.L. Steigerwald, A.P. Ramirez, Y.-U. Kwon, S.M. Stuczynski, L.F. Schneemeyer, J.V. Waszczak, and J. Zaanen, *Phys. Rev. Lett.* **71**, 1768 (1993).
- ³⁸A.C. Reber and S.N. Khanna, *Eur. Phys. J. D* **72**, 199 (2018).
- ³⁹C.-H. Lee, L. Liu, C. Bejger, A. Turkiewicz, T. Goko, C.J. Arguello, B.A. Frandsen, S.C. Cheung, T. Medina, T.J.S. Munsie, R. D'Ortenzio, G.M. Luke, T. Besara, R.A. Lalancette, T. Siegrist, P.W. Stephens, A.C. Crowther, L.E. Brus, Y. Matsuo, E. Nakamura, Y.J. Uemura, P. Kim, C. Nuckolls, M.L. Steigerwald, and X. Roy, *J. Am. Chem. Soc.* **136**, 16926 (2014).
- ⁴⁰A.C. Reber, V. Chauhan, and S.N. Khanna, *J. Chem. Phys.* **146**, 024302 (2017).
- ⁴¹Fenske Dieter and Ohmer Johannes, *Angew. Chem. Int. Ed. Engl.* **26**, 148 (1987).
- ⁴²O. Cador, H. Catey, J.-F. Halet, W. Meier, Y. Mugnier, J. Wachter, J.-Y. Saillard, B. Zouhoune, and M. Zabel, *Inorg. Chem.* **46**, 501 (2007).
- ⁴³S. Mandal, A.C. Reber, M. Qian, P.S. Weiss, S.N. Khanna, and A. Sen, *Acc. Chem. Res.* **46**, 2385 (2013).
- ⁴⁴E.S. O'Brien, J.C. Russell, M. Bartnof, A.D. Christodoulides, K. Lee, J.A. DeGayner, D.W. Paley, A.J.H. McGaughey, W.-L. Ong, J.A. Malen, X.-Y. Zhu, and X. Roy, *J. Am. Chem. Soc.* **140**, 15601 (2018).
- ⁴⁵B. Choi, K. Lee, A. Voevodin, J. Wang, M.L. Steigerwald, P. Batail, X. Zhu, and X. Roy, *J. Am. Chem. Soc.* **140**, 9369 (2018).
- ⁴⁶W.-L. Ong, E.S. O'Brien, P.S.M. Dougherty, D.W. Paley, C.F.H. Iii, A.J.H. McGaughey, J.A. Malen, and X. Roy, *Nat. Mater.* **16**, 83 (2017).
- ⁴⁷J.L. Shott, M.B. Freeman, N.-A. Saleh, D.S. Jones, D.W. Paley, and C. Bejger, *Inorg. Chem.* **56**, 10984

(2017).

⁴⁸E. Janssens, S. Neukermans, H.M.T. Nguyen, M.T. Nguyen, and P. Lievens, *Phys. Rev. Lett.* **94**, 113401 (2005).

⁴⁹H.T. Le, S.M. Lang, J.D. Haeck, P. Lievens, and E. Janssens, *Phys. Chem. Chem. Phys.* **14**, 9350 (2012).

⁵⁰X. Li, P. Claes, M. Haertelt, P. Lievens, E. Janssens, and A. Fielicke, *Phys. Chem. Chem. Phys.* **18**, 6291 (2016).

⁵¹J.U. Reveles, P.A. Clayborne, A.C. Reber, S.N. Khanna, K. Pradhan, P. Sen, and M.R. Pederson, *Nat Chem* **1**, 310 (2009).

⁵²H.T. Pham, L.Q. Ngo, M.P. Pham-Ho, and M.T. Nguyen, *J. Phys. Chem. A* **120**, 7964 (2016).

⁵³J.M. Goicoechea and J.E. McGrady, *Dalton Trans.* **44**, 6755 (2015).

⁵⁴X. Jin, V. Arcisauskaite, and J. E. McGrady, *Dalton Trans.* **46**, 11636 (2017).

⁵⁵S. Khanna, B. Rao, and P. Jena, *Phys. Rev. Lett.* **89**, 016803 (2002).

⁵⁶M.B. Abreu, A.C. Reber, and S.N. Khanna, *J. Phys. Chem. Lett.* **5**, 3492 (2014).

⁵⁷W.H. Blades, A.C. Reber, S.N. Khanna, L. López-Sosa, P. Calaminici, and A.M. Köster, *J. Phys. Chem. A* **121**, 2990 (2017).

⁵⁸D. Bista, A.C. Reber, V. Chauhan, and S.N. Khanna, *Chem. Phys. Lett.* **706**, 113 (2018).

⁵⁹D.E. Bergeron, A.W. Castleman, N.O. Jones, and S.N. Khanna, *Nano Lett.* **4**, 261 (2004).

⁶⁰M.P. Woodard, S.T. Akin, C.J. Dibble, and M.A. Duncan, *J. Phys. Chem. A* **122**, 3606 (2018).

⁶¹S. Veliah, K. Xiang, R. Pandey, J.M. Recio, and J.M. Newsam, *J. Phys. Chem. B* **102**, 1126 (1998).

⁶²Klaus Capelle, "A Bird's Eye View of Density-Functional Theory" Physics Institute and the Chemistry Institute of the University of São Paulo at São Carlos, Brazil, and at the VIII'th Summer School on Electronic Structure of the Brazilian Physical Society.